1957

Further studies on the strength of columns under combined bending:and thrust, Lehigh University, (1957)

T. V. Galambos

R. L. Ketter

Welded Continuous Frames and Their Components

INTERIM REPORT NO. 36

FURTHER STUDIES ON THE STRENGTH OF COLUMNS UNDER COMBINED BENDING AND THRUST

by

Theodore V. Galambos

and

Robert L. Ketter

This work has been carried out as a part of an investigation sponsored jointly by the Welding Research Council and the Navy Department with funds furnished by the following:

American Institute of Steel Construction
American Iron and Steel Institute
Column Research Council (Advisory)
Institute of Research, Lehigh University

Office of Naval Research (Contract No. 39303)
Bureau of Ships
Bureau of Yards and Docks

June, 1957

Fritz Engineering Laboratory
Lehigh University
Bethlehem, Pa.

Fritz Laboratory Report No. 205A.19

(Not for Publication)

TABLE OF CONTENTS

I. INTRODUCTION

The study of steel columns at Lehigh University has as one of its objectives the determination of the behavior of columns in welded continuous frames. This paper presents the results of a part of one phase of this overall investigation and deals specifically with the problem of the strength of columns subjected to two given conditions of loading. Results have been presented in interaction curve form and comparisons have been made with available test data. Approximate design equations have also been included.

The work leading up to this report is contained in the following published and unpublished papers:

1. Progress Report No. 6, "Column Strength Under Combined Bending and Thrust", (Ref. 6).

   In this report are presented the elastic limit interaction curve equations for the four conditions of loading illustrated in Figure 1. (Condition "a" - moments applied at both ends of the column producing double curvature; condition "b" - moment applied at one end, the other end held fixed; condition "c" - moments applied at both ends producing single curvature in the member; and condition "d" - moment applied at one end, the other end pinned.) This report also gives the fully plastic equation for a zero length member.

2. Progress Report "L", "Interaction Curves for Columns", (Ref. 9).

   The detailed derivations for the equations summarized in Progress Report No. 6 are presented in this paper.

3. Progress Report No. 10, "Plastic Deformation of Wide-Flange Beam-Columns", (Ref. 4).

   This report presents a method whereby the basic moment-curvature relationships including the influence of axial thrust and cooling residual stress can be obtained. A set of curves summarizing the findings of this study are included here in Fig. 3. Column strengths are also developed for a selected range of variables and predictions are compared with test results.

4. Progress Report No. 11, "Stability of Beam-Columns Above the Elastic Limit", (Ref. 11).

   Using the M-ϕ relationship developed in Progress Report No. 10, this paper presents a method whereby approximate maximum carrying capacities can be determined for a condition "c" type of loading (see Fig. 1).

In this report nondimensional interaction curves are developed for a wide-flange section. The two conditions of loading that have been considered are "c" and "d" (see Fig. 1). Three types of curves are presented. These are

a. Initial Yield Interaction Curves

b. Maximum Carrying Capacity Interaction Curves (neglecting the influence of residual stress).

c. Maximum Carrying Capacity Interaction Curves (Including the influence of a residual stress of the type shown in Fig. 2).

The interaction curves for each of these cases are shown in Figs. 4, 5, 6 and 7, 8 and 9.

Approximate equations for the ultimate carrying capacity of members containing residual stresses of the type shown in Fig. 2 are next developed. These formulas are kept as close as practicable to the theoretically developed interaction curves in the range of most frequently occuring practical cases.

In the final portion of the paper the theoretical curves are compared to experimental test results. The following sets of tests are used for comparison:

a. Massonnet's experiments in Belgium (Ref. 1).

b. Johnston and Cheney's experiments at Lehigh University (Ref. 8).

c. Wisconsin experiments for the Special Committee on Column Strength of the A.S.C.E. (Ref. 12).

d. Tests in the current Lehigh University Investigation (Ref. 10 and more recent results).

II. DEVELOPMENT OF THE INTERACTION CURVE

As stated in the preceding section, three types of interaction curves will be developed. The first of these is for the case of initial yielding in the member. (While these general equations have been developed elsewhere, Ref. 9, it was considered necessary for completeness to include them in this report.) The other two types that are considered are for the maximum carrying capacity; one that assumes no residual stress, and the other that assumes a residual stress of the magnitude and pattern shown in Fig. 2. Since the latter two cases are determined by numerical integration of a given moment-curvature relationship, and since the starting point for these calculations is the elastic limit deflection, the elastic deflection equations have also been included in the sections on initial yield.

1. Initial Yield Interaction Curves

a. Loading Condition "c" (pin-ended member subjected to equal end moments producing single curvature).

Timoshenko, on page 12 of his book on "Elastic Stability" (Ref. 5), gives the following equation for the deflection of an axially loaded member subjected to couples applied at each end. (For the nomenclature see Appendix A.)

$$y = \frac{M_b}{P}\left[\frac{\sin kx}{\sin kL} - \frac{x}{L}\right] + \frac{M_a}{P}\left[\frac{\sin k(L-x)}{\sin kL} - \frac{L-x}{L}\right] \quad \ldots\ldots (a)$$

For the case where $M_a = M_b = M_o$ and $P = P_o$, equation (a) reduces to

$$y = \frac{M_o}{P_o \sin kL}\left[\sin kx + \sin k(L-x) - \sin kL\right] \quad \ldots\ldots (b)$$

The interaction curve equation for this condition is developed on page 20 and 21 of Progress Report "L" (Ref. 9) and is as follows:

$$M_o = S\left[\sigma_y - \frac{P_o}{A}\right] \cos\frac{kL}{2} \quad \ldots\ldots\ldots\ldots\ldots\ldots (c)$$

Non-dimensionalizing this equation with respect to the moment that would just produce initial yielding in the member had it been subjected to pure moment (i.e. no thrust).

$$\frac{M_o}{M_y} = \frac{S}{M_y}\left[\sigma_y - \frac{P_o}{A}\right] \cos\frac{kL}{2} \quad \ldots\ldots\ldots\ldots\ldots\ldots (d)$$

But $M_y = S\sigma_y$ and $P_y = A\sigma_y$. Therefore,

$$\boxed{\frac{M_o}{M_y} = \left(1 - \frac{P_o}{P_y}\right) \cos\frac{kL}{2}} \quad \ldots\ldots\ldots\ldots\ldots\ldots (1)$$

For ease of computation Equation (1) can be rewritten in a slightly different form by noting that

$$\frac{kL}{2} = \frac{L}{2}\sqrt{\frac{P_o}{EI}} = \frac{L}{2}\sqrt{\frac{P_o}{EAr^2}} = \frac{1}{2}\frac{L}{r}\sqrt{\frac{P_o}{AE}}$$

$$= \frac{1}{2}\left(\frac{L}{r}\right)\sqrt{\frac{P_o\,\sigma_y}{A\,\sigma_y E}} \qquad = \frac{1}{2}\left(\frac{L}{r}\right)\sqrt{\frac{P_o}{P_y}\cdot\frac{\sigma_y}{E}}$$

or

$$\frac{kL}{2} = \frac{1}{2}\sqrt{\frac{\sigma_y}{E}}\left[\frac{L}{r}\sqrt{\frac{P_o}{P_y}}\right] \quad \ldots\ldots\ldots\ldots\ldots\ldots (e)$$

For an E value of 30,000,000 psi and σ_y of 33,000 psi, this reduces to

$$\frac{kL}{2} = (0.005491)\,\frac{L}{r}\sqrt{\frac{P_o}{P_y}} \qquad \ldots\ldots\ldots\ldots\ldots\ldots (f)$$

When substituted into equation (1)

$$\boxed{\frac{M_o}{M_y} = \left[1 - \frac{P_o}{P_y}\right] \cos\left((0.005491)\frac{L}{r}\sqrt{\frac{P_o}{P_y}}\right)} \qquad \ldots\ldots (1a)$$

This equation has been plotted on Fig. 4 in interaction curve form for slenderness-ratios ranging from 0 to 120 in increments of 20.

Since the deflected shape of the column axis at the time of initial yielding is necessary for later calculations, it is here further developed. Working with equation (b),

$$y = \frac{\frac{M_o}{M_y} \cdot M_y}{\frac{P_o}{P_y} \cdot P_y}\left[\frac{1}{\sin kL}\right]\left[\sin kx + \sin k(L-x) - \sin kL\right]$$

$$y = \left[\frac{\frac{M_o}{M_y}}{\frac{P_o}{P_y}}\right]\left(\frac{S}{A}\right) \qquad \left[\frac{\sin kx}{\sin kL} + \frac{\sin kL \cos kx - \cos kL \sin kx}{\sin kL} - \frac{\sin kL}{\sin kL}\right]$$

which gives

$$y = \left(\frac{S}{A}\right)\left[\frac{\frac{M_o}{M_y}}{\frac{P_o}{P_y}}\right]\left[\frac{\sin kx}{\sin kL} - 1 + \cos kx - \cot kL \sin kx\right] \ldots (g)$$

Note from equation (f) that if

$$kL = 0.010982 \frac{L}{r}\sqrt{\frac{P_o}{P_y}}$$

kx will similarly be

$$kx = 0.010982 \frac{x}{r}\sqrt{\frac{P_o}{P_y}} \qquad \text{.....(h)}$$

Substituting these expressions and the S/A value for the 8 WF 31* section into Equation (g) results in the following equation which contains only the variables L/r, x/r, y, M_o/M_y and P_o/P_y,

$$y = (3.010)\left[\frac{\frac{M_o}{M_y}}{\frac{P_o}{P_y}}\right]\left[\frac{\sin\left(0.010982\frac{x}{r}\sqrt{\frac{P_o}{P_y}}\right)}{\sin\left(0.010982\frac{L}{r}\sqrt{\frac{P_o}{P_y}}\right)} + \cos\left(0.010982\frac{x}{r}\sqrt{\frac{P_o}{P_y}}\right) - \left\{\cot\left(0.010982\frac{L}{r}\sqrt{\frac{P_o}{P_y}}\right)\right\}\left\{\sin\left(0.010982\frac{x}{r}\sqrt{\frac{P_o}{P_y}}\right)\right\} - 1\right] \qquad \text{.....(2)}$$

b. Loading Condition "d" (Pin-ended member subjected to end moment applied only at one end of member . See Fig. 1)

The interaction curve equation was developed on pages 9-13 of Progress Report "L" and is as follows:

$$M_o = S\left[\sigma_y - \frac{P_o}{A}\right]\sin kL$$

Dividing through by M_y and substituting the value of kL from Eq. (h)

$$\boxed{\frac{M_o}{M_y} = \left[1 - \frac{P_o}{P_y}\right]\sin\left(0.010982\frac{L}{r}\sqrt{\frac{P_o}{P_y}}\right)} \qquad \text{.....(3)}$$

* See discussion on page 14 for justification of the use of 8WF31 slope.

This equation has been plotted on Fig. 7 in interaction curve form for slenderness-ratios of 0, 80,100 and 120. It should be noted that equation (3) assumes that the maximum moment occurs away from the end of the member. When this is not the case and the applied end moment is the maximum moment along the member the interaction curve equation becomes a straight line as shown.

The deflection equation for this condition of loading is given on page 11 (Equation 18) of Ref. 5.

$$y = \frac{M_o}{P}\left(\frac{\sin kx}{\sin kL} - \frac{x}{L}\right) \quad \ldots\ldots\ldots\ldots\ldots\ldots\ldots (i)$$

Non-dimensionalizing, this becomes

$$y = \left(\frac{S}{A}\right)\left(\frac{\frac{M_o}{M_y}}{\frac{P_o}{P_y}}\right)\left[\frac{\sin kx}{\sin kL} - \frac{x}{L}\right] \quad \ldots\ldots\ldots\ldots\ldots\ldots (j)$$

or for the 8 WF 31 section

$$y = (3.010)\left[\frac{\frac{M_o}{M_y}}{\frac{P_o}{P_y}}\right]\left[\frac{\sin\left(0.010982\,\frac{x}{r}\sqrt{\frac{P_o}{P_y}}\right)}{\sin\left(0.010982\,\frac{L}{r}\sqrt{\frac{P_o}{P_y}}\right)} - \frac{x}{L}\right] \quad \ldots\ldots (4)$$

In each of the interaction curve figures that have been and will be presented there has also been given a scale (across the top and down the right hand side) for ec/r^2. That is, a line drawn from the origin through the ec/r^2 value in question will intersect the desired slenderness curve at the critical value of P_o/P_y. This follows from the fact that had the member been eccentrically loaded,

$$P\,e = M_o$$

or non-dimensionalizing

$$\frac{Pe}{S\sigma_y} = \frac{M_o}{M_y}$$

If the left hand side of this equation is multiplied by P_y/P_y

$$\frac{Pe}{S\sigma_y} \cdot \frac{A\sigma_y}{P_y} = \left(\frac{P}{P_y}\right)\left(\frac{e}{S/A}\right) = \left(\frac{P}{P_y}\right)\left(\frac{ec}{r^2}\right)$$

or

$$\left(\frac{P}{P_y}\right)\left(\frac{ec}{r^2}\right) = \frac{M_o}{M_y} \quad \ldots\ldots\ldots\ldots\ldots\ldots\ldots\ldots\ldots\ldots (k)$$

2. Interaction Curves for Maximum Carrying Capacity

The interaction curves for loading condition "c" neglecting residual stress are shown in Fig. 5. For the case of an assumed residual stress of the type and magnitude shown in Fig. 2, the curves are shown in Fig. 6. The corresponding interaction curves for loading condition "d" are shown in Figs. 8 and 9.

In the following discussion a method is presented for developing the curves shown for case "d". A similar method was used in the development of each of the curves. The numerical work is materially reduced for the condition "c" type of loading due to symmetry. A typical solution for this loading is shown in the Appendix of Progress Report R (Ref.7).

The problem is essentially as follows: for a given slenderness ratio and given axial thrust it is desired to construct a curve which defines the relationship between the applied end moment and resulting

end rotation as strains within the member become inelastic. It is further desired to take into account the residual stresses which are "locked-up" in the member due to rolling. (The presence of these residual stresses, their magnitude and distribution have been demonstrated in previous reports, Ref. 10,). Having defined this applied moment-resulting rotation relationship, the maximum carrying capacity will correspond to the uppermost point on this curve; that is, the point at which the derivation of the end moment with respect to the end rotation becomes zero.

Assumptions and limitations of the solution are

1. The moment-curvature relationship will be that shown in Fig. 3.
2. Failure will correspond to excessive bending in the plane of the applied moments; that is, in the plane of the web. (Failure due to combined bending and twist or due to local instability of the flange elements is not considered.)

The solution will be one of numerical integration of the given M-ϕ relationship. The systematized numerical integration procedure of Newmark (Ref. 3) has been used.

For ease of understanding an actual case will be computed. The problem for consideration has the following given conditions:

$P_o / P_y = 0.80$ $\quad (P_o = 0.80 \times 301 = 240.8^K)$

$L/r = 40$

8 WF 31 Section

The length corresponding to this assumed slenderness ratio is

$$L = 40\ (3.47) = 138.8 \text{ inches}$$

Subdividing this length into 8 equal divisions of λ each,

$$\lambda = 17.35 \text{ inches.}$$

For a first trial, assume that the member is subjected to an end moment M_o such that $M_o / M_y = 0.20$. The elastic deflection according to equation (4) would then be

$$y = (3.010)\ \frac{0.20}{0.80}\ \frac{\sin\ (0.010982)\ (40)}{\sin\ (0.010982)\ (40)}\ \frac{0.80}{0.80} - \frac{x}{L}$$

or

$$y = (0.7525)\ \frac{\sin\ 1.188\ \frac{x}{L}}{0.9276} - \frac{x}{L} \quad \ldots\ldots\ldots\ldots\ldots (5)$$

"x" is measured from the M_o end of the member.

A tabular solution of Equation (5) is given in Appendix C. These deflection values will be used in the first cycle of the numerical integration. As stated previously, the column has been subdivided into 8 equal parts 17.35 inches in length. In line "a" the moments due to M_o are listed for each point. The assumed deflections are indicated in line "b". For the first approximation the "initial yield" solution calculated in Appendix C is used. For each successive numerical integration cycle, the final deflections of the previous cycle are used until convergence is reached. In line "c" the moment $P_o y$ is shown; in line "d" is given the sum of the moments in lines "a" and "c". This total moment is then transformed into non-dimensional form by dividing by M_y (M_y=904.2 in. kips for the 8WF31 section). This is shown in line "e". In line "f" the concentrated

angle changes are listed. These were obtained from an enlarged version of the M/M_y versus ϕ/ϕ_y curves of Fig. 3. The $P/Py = 0.8$ curve was used.

Lines "g" and "h" show the performance of the usual numerical integration process. For example, in line "g" the values of line "f" have been added in consecutive order. Multiplying by the factor shown in the right hand column $(\text{i.e. }, \lambda\phi_y)$ will give the slope at the midpoint of each of the segments. In a similar manner line "h" is obtained. It should be noted, however, that line "h" indicates a deflection at point 9, the right hand end of the beam-column. Since there is no deflection at that point a rigid body rotation is performed and proportional correction factors are computed in line "i". The sum of lines "h" and "i" give the final deflection in terms of the multiplication factor for this cycle of integration. Multiplying these values by $\lambda^2\phi_y$ (i.e., $17.35^2 \times 0.000275 = 0.0828$) will give the final deflection in inches.

As would be expected, the final deflections do not correspond to the assumed ones shown in line "b". Therefore other cycles of integration must be carried out. The initial and the final deflections for the fourth cycle are shown at the bottom of Appendix 4. It should be noted that the two deflections varied at the most 0.001 inches. For most of the calculations three cycles of integration were sufficient.

The true deflected configuration of the column has now been obtained for the given ratio of Po/P_y and L/r and for the

assumed M_o/M_y. The next step in the procedure is to compute the rotation at the applied moment end of the member. This is calculated from the following equation :

$$\theta_A = \frac{4\,\delta_B - \delta_C}{2\lambda}$$

which, as shown in Appendix E, assumes that the deflection curve (considering only the last two segments) can be represented by a parabola. The deflections δ_B and δ_C are the deflections at sections 2 and 3 on the column. From Appendix D these were shown to be δ_B = 0.070 inches and δ_C = 0.113 inches. It therefore follows that

$$\theta_A = \frac{4(0.070) - 0.113}{2(17.35)} = 0.00481$$

For a range of increasing values of M_o/M_y the end slope (θ_A) is determined. These are then plotted as shown in Fig. 10. The point on this graph at which the M_o/M_y value becomes a maximum corresponds to the maximum carrying capacity of the member (with P_o/P_y = 0.80 and L/r = 40). This point of collapse is characterized by the fact that at this value of end moment the numerical integration process begins to give divergent results. For the case in question M_o/M_y (max) = 0.233. Since the properties of this section were based on average measured values for the standard 8 WF 31 section, and since the corresponding shape factor, f, of the section was 1.09 (Ref. 4), this critical value of end moment could be non-dimensionalized with respect to the fully plastic moment by dividing by the shape factor. That is,

$$\frac{M_o}{M_p}_{(max.)} = \frac{0.233}{1.09} = 0.214$$

The curves shown in Figs. 5, 6, 8 and 9 were all computed, point by point, by this laborious method. A point of collapse was found for each increment of load and slenderness.

3. Discussion of the Interaction Curves

It should be emphasized that the interaction curves for maximum carrying capacity as shown in Figs. 5, 6, 8 and 9 were computed for the 8 WF 31 section. However, since it is reasonable to assume that as the shape factor of a member increases, the strength of the corresponding beam-column should also become larger; and since the shape factor used in the calculations was 1.09 (the lowest value for rolled WF and I shapes), use of these curves for other sizes should give conservative strength predictions.

For steels of different yield strength than 33 ksi, the values of slenderness ratios, L/r, should be modified by the factor $\sqrt{33/\sigma^*_y}$ as indicated. This will ensure that in the non-dimensional form, the intersection of the Euler curve and yield point of the material will always correspond to the correct slenderness value.

To make the graphs more useful when eccentricity values (ec/r^2) are given instead of end moment, values of ec/r^2 are also given on these figures.

---

* σ_y is the yield stress level of the material in question.

In outward appearance the curves for residual stress and without residual stress are very similar with the values being lower for the case with residual stress. The actual magnitude of this reduction is dependent on the condition of loading, slenderness ratio and Po/P_y or ec/r^2 value as shown in the diagrams.

III. APPROXIMATE DESIGN EQUATIONS

To facilitate the work of the designer, there are developed in this section, for various ranges of variables, approximate equations to the maximum strength interaction curves presented in the preceding chapter. Only the interaction curves including the influence of residual stress are considered.

The assumptions and limitations on these equations will be the same as for the interaction curves themselves; that is, the cross-section is assumed to be of the wide-flange type (in the strictest sense an 8 WF 31) and further that it is bent about its strong axis; the material is A-7 mild structural steel having a minimum yield stress level of 33 ksi, and the member is assumed to fail due to excessive bending in the plane of the applied moments (i.e. the plane of the web).

It should be re-emphasized that failure due to combined bending and twist has not been considered. While most laboratory columns fail in such a manner, a majority of the members found in practice are restrained in their weak direction by wall systems, etc. For these and other cases where adequate lateral support is provided, the derived equations directly apply. Local instability of flange elements has also not been considered. The problem is not considered to be of major concern for presently rolled shapes.

1. Axial Load Only

In Fig. 11 is shown the column curve for pure axial thrust which includes the influence of residual stress. If it is assumed that the range of slenderness in question is $0 \leq (L/r) \leq 120$, then the following approximate equation will define the relationship between

the axial thrust ratio (P_o / P_y) and slenderness ratio, (L/r), see Appendix F:

$$\frac{P_o}{P_y} = 1 - \frac{1}{3{,}500{,}000}\left(\frac{L}{r}\right)^3 + \frac{1}{32{,}000}\left(\frac{L}{r}\right)^2 - \frac{1}{358}\left(\frac{L}{r}\right) \quad \ldots\ldots(7)$$

This equation is shown as a dashed line in Fig. 11.

If it is desired to approximate only that portion of the curve below the Euler curve (i.e. $L/r \leq 112$), then the simpler expression

$$\frac{P_o}{P_y} = 1 - \frac{1}{111{,}000}\left(\frac{L}{r}\right)^2 - \frac{1}{645}\left(\frac{L}{r}\right) \quad \ldots\ldots\ldots\ldots\ldots(7a)$$

may be used.

Tabulated values of P_o/P_y versus L/r are given in Appendix F.

2. Approximate Interaction Equation for Condition "c" Loading

Assuming as in the case of pure axial thrust that L/r will not exceed 120 and further that $P_o/P_y \leq 0.6$ an equation of the type

$$\frac{M_o}{M_p} = 1 - \alpha\frac{P_o}{P_y} - \beta\left(\frac{P_o}{P_y}\right)^2 \quad \ldots\ldots\ldots\ldots\ldots(8)$$

can be made to approximate the curves shown in Fig. 6. α and β are assumed to vary with the slenderness according to the general equations

$$\left.\begin{aligned} \alpha &= a_1 + a_2\left(\frac{L}{r}\right) + a_3\left(\frac{L}{r}\right)^2 + a_4\left(\frac{L}{r}\right)^3 \\ \beta &= b_1 + b_2\left(\frac{L}{r}\right) + b_3\left(\frac{L}{r}\right)^2 + b_4\left(\frac{L}{r}\right)^3 \end{aligned}\right\} \quad \ldots\ldots\ldots\ldots(8a)$$

Then as shown in Appendix F (section 2),

$$\left.\begin{aligned} \alpha &= 0.420 + \frac{(L/r)}{69} - \frac{(L/r)^2}{29,000} + \frac{(L/r)^3}{1,164,000} \\ \text{and} \\ \beta &= 0.770 - \frac{(L/r)}{58.1} + \frac{(L/r)^2}{8,700} - \frac{(L/r)^3}{606,000} \end{aligned}\right\} \quad \ldots\ldots\ldots\ldots (8b)$$

A comparison between the "measured" and the approximate values for α and β is shown in Fig. 12.

Fig. 13 compares the resulting approximate equations with the interaction curves of Fig. 6. Again to facilitate their use, values of α and β have been tabulated for various slenderness ratios from 0 to 120 (Table II).

3. Approximate Interaction Equation for Condition "d" Loading

The following type of approximate equation was developed for loading condition "d" (see Appendix F - section 3):

$$\frac{Mo}{Mp} = \alpha \frac{Po}{Py} + \beta \quad \ldots\ldots\ldots\ldots\ldots\ldots\ldots\ldots (9)$$

Here, as before α and β are assumed to vary with slenderness, and as shown in Appendix F - (section 3)

$$\left.\begin{aligned} \alpha &= -1.110 - \frac{(L/r)}{189} + \frac{(L/r)^2}{8,889} - \frac{(L/r)^3}{720,000} \\ \text{and} \\ \beta &= 1.133 + \frac{(L/r)}{3080} + \frac{(L/r)^2}{185,000} \end{aligned}\right\} \quad \ldots\ldots\ldots\ldots (9a)$$

Plotting Equations (9) and (9a) versus the interaction curves of Fig. 9 (see Fig. 15), it is noted that for lower values of (L/r) the approximate Equation is conservative; whereas, for larger values, too great a moment capacity is predicted. Neglecting the influence of strain-hardening, it is known that the maximum moment a beam can sustain when subjected to pure moment is its fully plastic value. A value of $M_o/M_p = 1.0$ should therefore be the absolute maximum that the approximate relationship can take. Due to strain-hardening, it has been observed from test results that for this loading condition the presence of a thrust of 0.12 P_y will not reduce the moment capacity below this fully plastic value, M_p (see Table 8, Appendix G). Therefore, Equations (9) and (9a) are the approximate interaction equations providing the predicted $M_o/M_p \leq 1.0$. When these equations predict a value of $M_o/M_p \geq 1.0$, the 1.0 value should be used.

4. Summary of Approximate Equations

a. Axial Load only:

$$\frac{P_o}{P_y} = 1.0 - \frac{1}{3{,}500{,}000}\left(\frac{L}{r}\right)^3 + \frac{1}{32{,}000}\left(\frac{L}{r}\right)^2 - \frac{1}{358}\left(\frac{L}{r}\right)$$

Values of P_o/P_y for $0 < L/r < 120$ are tabulated in Table 1, Appendix F. The equation is valid from $0 < L/r < 120$.

b. Case "c" Loading

$$\frac{M_o}{M_p} = 1.0 - \frac{P_o}{P_y}\left(\alpha + \frac{P_o}{P_y}\beta\right)$$

Values of α and β for $0 \leq L/r \leq 120$ are given in Table 2 of Appendix F. The equation in not valid for $P_o/P_y > 0.6$.

c. Case "d" Loading

$$\frac{Mo}{M_p} = \alpha\left(\frac{Po}{P_y}\right) + \beta$$

Values of α and β for $0 < L/r < 120$ are given in Table 3 of Appendix F. The equation is not valid for $Po/P_y > 0.6$. Where the equation predicts a value of $Mo/M_p > 1.0$, the value $M_o/M_p = 1.0$ should be used.

An alternate (less precise) approximation,

$$\frac{M_o}{M_p} = \frac{\alpha - P/Py}{\alpha - 0.12} \quad ,$$

could be used for this loading condition. It should be pointed out, however, that if values of the constants are to be tabulated; the more precise two constant equations will be no more difficult to use than the one constant equation.

IV. COMPARISON OF THEORETICAL PREDICTIONS WITH EXPERIMENTAL RESULTS

In developing the maximum strength interaction curves of section II of this report, it was necessary to make certain assumptions. (The major one of these was that lateral torsional buckling will not occur.) In this section, these predictions of strength will be compared with test results.

The following experimental data will be used for comparison:

a. Johnston and Cheney's tests (Ref. 8),

b. Massonnet's tests (Ref. 1),

c. Tests in the current Lehigh series (Ref. 6 plus more recent results), and

d. Wisconsin tests (Ref. 12).

1. Tests of Johnston and Cheney.

Johnston and Cheney performed a series of column tests at Lehigh University in the early 1940's. Their findings are recorded in Ref. 8.

In total 93 column tests were carried out; 89 were made on 3 I 5.7 sections and 6 were made on 6 WF 20 sections. Columns were tested by both concentric and eccentric application of the axial thrust; however, the column tests under pure axial load cannot be compared with the interaction curve since their end conditions were such that they failed by column buckling about the weak axis. The tests which can be compared with the derived curves are tabulated in Table 4 of Appendix G. With the exception of the value P_o/P_y, all values shown in this table have been reproduced

from Table No. V (p.20) of Ref. 8. The test numbers refer to the original test number designations. The column headed by "Member" indicates whether the section was a 3 I 5.7 (Marked - I), or a 6 WF 20 (marked - II). Lot 1 in the material column signifies a steel with a yield strength of 42.4 ksi, whereas lot 2 is for one having a value 40.8. The yield strength of lot 3 was 39.8 ksi. Appendix G lists the section and material properties of the columns. The eccentricity ratios are also given. It should be pointed out that, due to the manner of load application (through knife-edges), the members were pin-ended in their strong direction and essentially fixed in their weak direction.

These tests correspond to a condition "c" type of loading, and Figs. 16 and 17 show the comparison of the test results with the theoretical predictions. (The elastic limit solution is shown as a dotted line, the ultimate strength curve neglecting residual stress is a solid line, and the ultimate strength curve including residual stress, $\sigma_{RC} = 0.3\,\sigma_y$, is a dot-dash line. Slenderness ratios were adjusted to account for the difference in yield stress level.

Johnston and Cheney report that the "columns loaded eccentrically to produce bending in the strong direction usually failed by plastic lateral-torsional buckling, after initially passing the yield point in the case of the shorter columns, and somewhat below the yield point in the longer columns."

The higher final strengths of the short columns (L/r =22, see Figs. 16 and 17) can be explained by the action of strain-hardening, which was neglected in the calculations of the

interaction curves of section II. The columns with a high L/r (see Figs. 16 and 17) failed below the predicted values. For these columns lateral torsion has resulted in a decrease in the ultimate carrying capacity of the member.

2. Tests of Massonnet

In April 1956 Massonnet reported on a series of column tests which were conducted in Belgium (Ref. 2) A total of 95 tests were performed. The cross-sections considered were the DIE 10, DIE 20 and PN 22 profiles. The first two of these are geometrically similar to the American wide-flange shapes whereas the last is a narrow flange, rail-like, continental profile similar to the American I shaped section. Since the interaction curves of section 2 were developed for the wide-flange type of cross-section, the test results for the PN 22 section are not directly applicable. (The shape factor for the PN 22 section; i.e., the ratio of the initial yield moment to the fully plastic moment, is much greater than that of the DIE 10 and 20.)

It should here be observed that Massonnet's test columns were pinned at the ends in both directions since they were provided with almost frictionless, and almost perfectly hydraulically seated, steel balls. For such end conditions, the possibility of lateral-torsional buckling is most pronounced.

Three types of loading were used in these tests:

a. $e_2/e_1 = +1$; (e_1 and e_2 are end eccentricities of load application) this would correspond to a condition "c" type of loading.

b. $e_2/e_1 = 0$, i.e. $e_2 = 0$. This case corresponds to a type "d" condition of loading.

c. $e_2/e_1 = -1$, i.e. equal moments are applied at each end of the member in a manner which produces double curvature. This would correspond to a condition "a" type of loading.

Massonnet has in all cases applied an eccentricity of the axial thrust in the plane of the web (i.e. strong axis bending). In stating the program and in tabulating the results, however, ha has listed the slenderness ratios in the weak direction. Since the interaction curves developed in section two of this report consider only the behavior of the member in the plane of the applied moments, it is necessary that these values be referred to the strong direction. The test series as listed by Massonnet covers a range of slenderness, (L/r_y), from 40 to 175, with respect to the weak direction. This would correspond to an L/r_x from approximately 24 to 110.

The columns with the higher slenderness values were the DIE-10 sections (nominal $L/r_y = 130$ and 175, nominal $L/r_x = 82$ and 110.) These were the lighter sections and had a nominal area of 20.78 cm^2 (3.24 $in.^2$) as compared to 57.03 cm^2 (8.85 $in.^2$) for the DIE-20.

The eccentricity ratios for each increment of length were, in general,

$$\frac{ec}{r_x^2} = 0.5,\ 1.0 \text{ and } 3.0.$$

Massonnet denotes this ratio by the symbol "m" where

$$m = \frac{e}{\rho_x},$$

e being the end eccentricity of load application and ρ_x the core radius. Since the core radius can be expressed in terms of the radius of gyration as

$$\rho_x = \frac{2r_x^2}{d}$$

it can be shown that (note that c = d/2)

$$m = \frac{ec}{r^2}$$

In tables 6 and 7 of Appendix G, the test results are tabulated. These tables are taken largely from Table 8, pages 58, 59 and 60 of Reference 2. The test numbers are the original test number designation.

The area for each section was measured and reported in the paper; however, no individual measurements of the yield strength level were given. The value of P_y was therefore determined by multiplying the measured areas by 26.875 tons per square centimeter (1 metric ton = 1000 kg) for the DIE 10 section, and by 24.056 tons per square centimeter for the DIE 20 section. These values of the yield stress are average values, determined by coupon tests.

The value of P_o is the maximum reported load each column sustained. The slenderness ratios were determined as shown in Tables 6 and 7, and these were then reduced as in the other cases for comparison purposes to correspond to a 33 ksi yield-strength steel. The adjustment was made according to the equation:

$$\left(\frac{L}{r}\right)_{adj.} = \frac{L}{r}\sqrt{\frac{33}{\sigma_y^*}}$$

where

for DIE 10: $\sigma_y^* = 26.375$ tons/cm^2 = 38.2 ksi

for DIE 20: $\sigma_y^* = 24.056$ tons/cm^2 = 34.2 ksi

In Fig. 18, these test results are compared to each of the three interaction conditions discussed previously for a condition "c" type of loading. It will be noted that the test values deviate markedly from the predicted values. This is due to lateral torsional buckling which is more-or-less insured by the pin-ended condition in the weak direction. The Euler curve in the weak direction has also been shown to afford a better "feeling" of the closeness of this column buckling condition.

Fig. 19 indicates the correlation between predicted strength and experimental result for those members tested under a condition "d" type of loading. As would be expected, these results lie closer to the predicted cases than did those for condition "c" loading, since the problem of lateral-torsional buckling is not so severe. None the less, there is a marked influence of lateral buckling on the column strength. In this figure, there has also been shown the Euler column curve in the weak direction.

3. Tests in the Lehigh Series

Table 8, Appendix G lists certain of the tests that have been carried out in the present Lehigh Investigation and compares their results to predictions based on this report. A majority of the

results listed were taken from Ref. 6; however, there have been included the results of several more recent tests. The end conditions in each of these tests are pin-ended in the strong direction and fixed in the weak.

Since the majority of the members tested are in a range where the interaction curves converge to a point (i.e. for low values of Po/Py, all values of Mo/My approach the value 1.0), most of these test results have not been shown on graphs. While these ratios of thrust to moment at collapse are typical of those developed in single story portal frames, they do not afford a comparison over too wide a range of variables. For the pure axial load tests, however, Fig. 20 shows the correlation with predicted strength. An additional test by Huber (Ref. 10) (4WF13, L/r = 130) has been included to extend the range of coverage. It will be noted from Table 8 that experimental results have been tabulated with respect to two values of yield stress. The first of these, σ_y = 40 ksi, is that average value determined from tension coupon tests. The second tabulation is for an adjusted yield stress level which varies according to the section in question. As shown in Ref. 13, tension coupons tested at normal laboratory rates over estimate the true static yield stress level of the section. Assuming that the average values shown in Ref. 13 are correct, the adjusted non-dimensional values are made according to

8WF31 $\quad \sigma_y(\text{static}) = (0.92)\,\sigma_y(\text{coupon})$

4WF13 $\quad \sigma_y(\text{static}) = (0.97)\,\sigma_y(\text{coupon})$

The correlation between the test results for the axially load members, interpreted in the manner described above, is quite good.

4. Test in the Wisconsin Series

Ref. 12 describes a series of column tests that were carried out in the late 1920's at the University of Wisconsin. Rolled, built-up and tied columns were tested, and in Table 9 are listed those tests which can be compared with the loading condition "c" curves developed in section II of this report. The members tested were 8 H 32 shapes and corresponded to the modern 8 WF 31, which was used as a basis for calculations in this report. A constant value of $ec/r^2 = 1.0$ was used in each of the tests. End conditions were such that the member was essentially pinned in the strong direction and fixed in the weak.

These results are shown on Fig. 21. Tests H-1, H-2, and H-3 confirm the theoretical curve, whereas the tests with high L/r values fall below the predicted strengths. While the exact manner in which the members failed is not indicated in the report, it is reasonably safe to assume that these members failed by lateral-torsional buckling.

Since the members of this series of tests were geometrically similar to those of Massonnet's, the influence of pin-endedness versus fixed-endedness in the weak direction can be seen by comparing the test results of Figs. 18 and 21.

V. SUMMARY AND CONCLUSIONS

In this report there have been developed for two loading conditions ("c" and "d"--see Figure 1), interaction curves for predicting the strength of wide-flange beam columns bent about their strong axis. Three types of solutions were obtained. The first of these was the initial yield solution, (Fig. 4 and 7) the second was for maximum strength neglecting the influence of residual stress, (Figs. 5 and 8) and the third was for maximum strength including the influence of an assumed residual stress distribution (see Fig. 2). (Figs. 6 and 9) While strong axis bending was assumed, the solution did not take into account the possibility of lateral-torsional buckling. It should be noted, however, that while most test columns fail in this manner, a majority of the members found in practice are laterally restrained along their length by wall systems, bracing, etc. For these or other cases where adequate lateral restraint is provided, the solutions of this report directly apply.

Because of the large amount of numerical work required to obtain the maximum strength interaction curves, it was necessary to select a section for computation. Since the 8 WF 31 section has one of the lowest shape factors of any of the sections rolled, it was selected. The use of the resulting curves for other cross-sections will result in conservative strength predictions.

To facilitate analysis and design, approximate analytical expressions were developed for the maximum strength solutions

including the influence of residual stress. (Figs. 11, 13 and 15) Constants for these expressions are tabulated in Appendix F as Tables 1, 2 and 3.

In the last part of the report the theoretical curves are compared with test results. Four series of experiments were considered and graphs indicating the correlation were given. (Figs. 16-21) In general, as slenderness increased, there resulted a decrease in the carrying capacity of the member over that predicted herein. This tendency was further exaggerated when the member was also pin-ended in its weak direction. (Note, for example, the decrease in strength of Massonnet's columns over those of the Wisconsin series.) In all of these cases, failure was due to lateral-torsional instability. They indicate the seriousness of this problem in predicting the strength of laboratory test columns. Further work is currently underway.

VI. ACKNOWLEDGMENTS

This study was part of the general research program "Welded Continuous Frames and Their Components", being carried out at Fritz Engineering Laboratory, Lehigh University, Bethlehem, Pennsylvania under the general direction of Dr. Lynn S. Beedle. The investigation is sponsored jointly by the Welding Research Council and the Department of the Navy with funds furnished by

The American Institute of Steel Construction

American Iron and Steel Institute

Column Research Council (Adviser)

Office of Naval Research

Bureau of Ships

Bureau of Yards and Docks

Professor William J. Eney is Director of Fritz Engineering Laboratory and Head of the Department of Civil Engineering.

VII. REFERENCES

1. Massonnet, C., and Campus, F., "Correspondence on the 'Stauchion Problem in Frame Structures Designed According to Ultimate Carrying Capacity' by Horne, M. R." Proc. Inst. of Civil Engrs. par III, Vol. 5, pp.558-571, August,1956.

2. Massonnet, C. and Campus, F., "Recherchez sur le Flambent de Colonnes en Acier A37, a profil en double Te, sollicitees obliquement" I.R.S.I.A. Bulletin No. 17, April 1956.

3. Newmark, N.M., "Numerical Procedures for Computing Deflections, Moments and Buckling Loads." Transaction of the ASCE, Vol. 108, 1943, pp. 1161-1234.

4. Ketter, R.L., Kaminsky, E.L., Beedle, L.S., "Plastic Deformation of Wide Flange Beam-Columns". ASCE Proceedings Separate No.330, 1953.

5. Timoshenko, S., "Theory of Elastic Stability", McGraw-Hill Book Co., New York, (1936).

6. Ketter, R.L., Beedle, L.S., and Johnston, B.G., "Column Strength Under Combined Bending and Thrust", Progress Report No. 6, Welding Journal Research Supplement, Dec. 1952.

7. Ketter, R.L., and Beedle, L.S. "Moment Rotation Characteristics of Beam Columns", Progress Report R (F.L.), Nov. 1952.

8. Johnston, B.G., and Cheney, L. "Steel Columns of Rolled Wide Flange Section" Progress Report No. 2, AISC, Nov. 1942..

9. Ketter, R.L., and Beedle, L.S. ,"Interaction Curves for Columns",Progress Report L (F.L.), April, 1951.

10. Huber, A.W., "The Influence of Residual Stress on the Instability of Columns", Lehigh University Dissertation, May 1956.

11. Ketter, R.L., "Stability of Beam Columns Above the Elastic Limit" ASCE Sep. 692, Vol. 81, May 1955.

12. "Second Progress Report of the Special Committee on Steel Columns", Paper No. 1789, ASCE Transactions, Vol. 95, 1931.

13. Gozum,A.T., and Huber, A.W., "Material Properties, Residual Stresses and Column Strength", Fritz Engineering Report No. 220A.14, May, 1955 (Revised Nov. 1955).

A P P E N D I X

Appendix A

Nomenclature

A	Area of cross-section ($in.^2$)
E	Modulus of elasticity (E= 30,000 ksi for A-7 steel)
I	Moment of inertia about the x-x axis ($in.^4$)
L	Length of the member (inches)
M	Moment (inch-kips)
M_o	Applied moment at the end of the member (inch-kips)
$M_p = \sigma_y A$	Moment corresponding to full plasticity of the section (inch-kips)
$M_y = \sigma_y S$	Moment corresponding to initial yield under pure moment (inch-kips)
P, P_o	Applied axial load (kips)
$P_y = \sigma_y A$	Load corresponding to the yielding of a short column (kips)
S	Section Modulus about the x-x axis ($in.^3$)
Z	Plastic Modulus about the x-x axis ($inches^3$)
b	Width of flange
c	Distance from centroid to outer fiber (inches)
d	Depth of member
e	Eccentricity (inches)
$k = \sqrt{P/EI}$	A parameter, from page 2 of Reference 5.
r	Radius of gyration about the x-x axis (inches)
t	Thickness of flange
w	Thickness of web
x	A distance along the axis of the member (inches)
y	Deflection (inches)
ec/r^2	Eccentricity ratio
L/r	Slenderness-ratio

Nomenclature (cont'd)

α, β	Non-dimensional constants
δ	Deflections of specific stations along the member (in.)
θ	End rotation (radians)
$\phi_y = \frac{2\sigma_y}{dE}$	Unit rotation corresponding to initial yield under pure moment
λ	A distance which is evenly divisible into the length of the member (inches)
σ_y	Yield point stress. (Assumed to be 33 ksi for A-7 steel).

Appendix B

Sectional Properties of an 8 WF 31 Section.

From AISC Handbook:

d = 8.00 in	A = 9.12 in^2	Iy = 37.0 in^4
b = 8.000 in	Ix = 109.7 in^4	Sy = 9.2 in^3
t = 0.433 in	Sx = 27.4 in^3	y = 2.01 in
w = 0.288 in	x = 3.47 in	c_x = 4.00 in

$$\phi_y = \frac{2\sigma_y}{Ed} = \frac{(2)\ (33)}{(30{,}000)(8.00)} = 0.000275 \text{ radians}$$

$$M_y = S\sigma_y = (27.4)\ (33) = 904.2 \text{ in kips}$$

$$P_y = A\sigma_y = (9.12)\ (33) = 301^K$$

$$\frac{r_x^2}{c_x} = \frac{(3.47)^2}{4.00} = 3.010 \text{ in}$$

$$kL = \sqrt{\frac{\sigma_y}{E}}\left[\frac{L}{r}\sqrt{\frac{P_o}{P_y}}\right] = 0.010982\ \frac{L}{r_x}\sqrt{\frac{P_o}{P_y}}$$

$$kx = 0.010982\ \frac{x}{r}\sqrt{\frac{P_o}{P_y}}$$

Appendix C

A tabulated solution of Equation 6

$$y = 0.7525\left(\frac{\sin 1.188\ x/L}{0.92762}\right) - \left(\frac{x}{L}\right)$$

Position	"x" (inches)	x/L	1.188 x/L	sin 1.188 x/L	$\frac{\sin 1.188\ x/L}{0.92762}$	$\left(\frac{\sin 1.188\ \frac{x}{L}}{0.92762}\right) - \left(\frac{x}{L}\right)$	"y" (inches)
1	0	0	0	0	0	0	0
2	17.35	0.125	0.1485	0.14796	0.160	0.035	0.026
3	34.7	0.250	0.2970	0.29265	0.315	0.065	0.049
4	52.05	0.375	0.4455	0.43091	0.465	0.090	0.068
5	69.4	0.500	0.5500	0.52269	0.563	0.063	0.047
6	86.75	0.625	0.6875	0.63460	0.684	0.059	0.044
7	104.1	0.750	0.825	0.73454	0.792	0.042	0.032
8	121.45	0.875	0.9625	0.82062	0.885	0.010	0.008
9	138.8	1.000	1.1880	0.92762	1.000	0	0

For the case of

$M_o = 0.20\ \ M_y = (0.20)\ (904.2) = 180.84^{"K}$

The end shear (i.e. the horiz. Reaction is $\frac{Mo}{L} = \frac{180.84}{138.8} = 1.303^K$

Then the moment at each position is the following:

Position	1	2	3	4	5	6	7	8	9
"x"	0	17.35	34.7	52.05	69.4	86.75	104.1	121.45	138.8
$M_o - \frac{Mo}{I}x$	181	158	136	113	90	68	45	22	0

Appendix D

$L/r = 40$
$P_o/P_y = 0.8$
$M_o/M_y = 0.2$

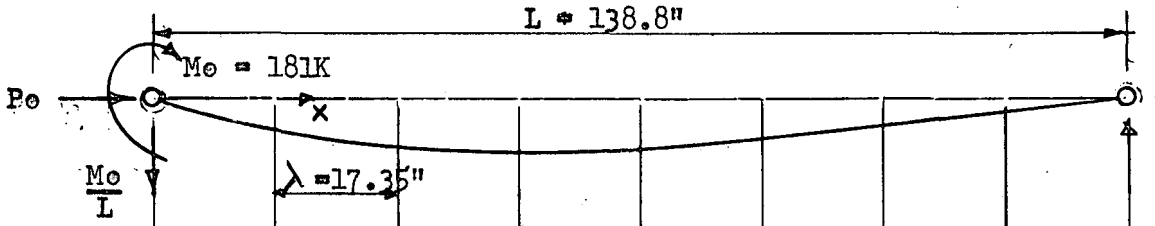

	1	2	3	4	5	6	7	8	9	MF	Notation
a	181	153	136	113	90	68	45	23	0		Moment due to M_o
b	0	0.026	0.049	0.068	0.047	0.044	0.032	0.008	0		Assumed deflection
c	0	5	10	14	10	9	7	2	0		Moment due to P_o
d	181	163	146	127	100	77	52	25	0		Total Moment (a + c)
e	0.200	0.180	0.161	0.140	0.111	0.085	0.058	0.028	0		M_x / M_y
f	0.350	0.290	0.250	0.210	0.151	0.119	0.083	0.045	0	ϕ_y	Concentrated angle changes
g		0.350	0.640	0.890	1.100	1.251	1.370	1.453	1.498	$\lambda\phi_y$	Slope
h	0	0.350	0.990	1.880	2.980	4.231	5.601	7.054	8.552	$\lambda^2\phi_y$	Deflection
i	0	1.069	2.138	3.207	4.276	5.345	6.141	7.483	8.552	$\lambda^2\phi_y$	Correction to deflection
j	0	0.719	1.143	1.327	1.296	1.114	0.540	0.429	0	$\lambda^2\phi_y$	Final deflection
k	0	0.060	0.095	0.110	0.107	0.092	0.045	0.036	0		Final deflection in inches

(1st Trial)

a	0	0.069	0.112	0.131	0.129	0.112	0.081	0.043	0		Assumed deflection 4th trial
k	0	0.070	0.113	0.132	0.130	0.112	0.082	0.043	0		Final deflection 4th trial

Derivation of the end slope equation:

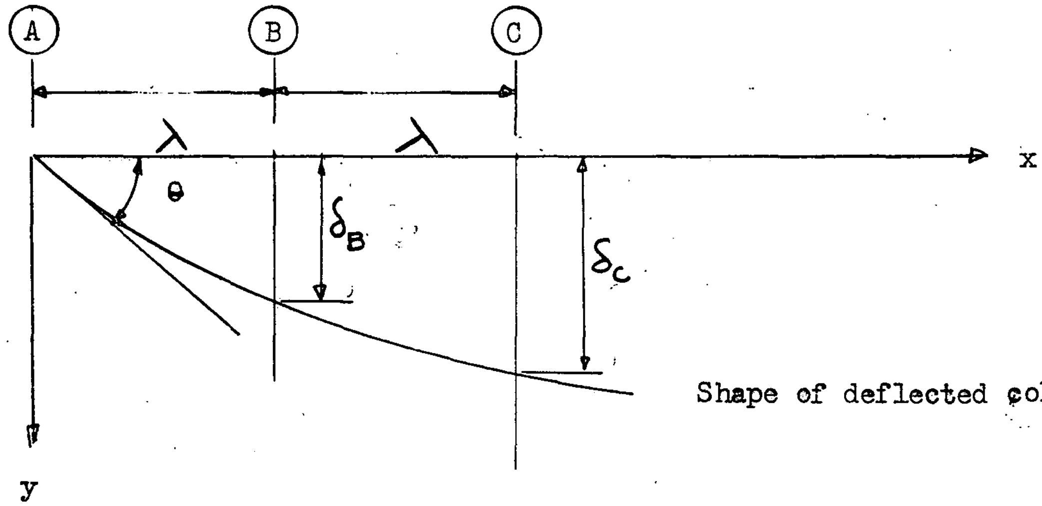

Shape of deflected column

Assume that the deflected shape of the column is a parabola of the form

$$y = Ax^2 + Bx + C$$

Boundary conditions: @ $x = 0$ $y = 0$

@ $x = \lambda$ $y = \delta_B$

@ $x = 2\lambda$ $y = \delta_C$

1.) $0 = C$

2.) $\delta_B = A\lambda^2 + B\lambda \longrightarrow A = \dfrac{\delta_B - B\lambda}{\lambda^2}$

3.) $\delta_C = 4A\lambda^2 + 2B\lambda$

$\delta_C = 4\delta_B - 4B\lambda + 2B\lambda$

$$B = \frac{4\delta_B - \delta_C}{2\lambda}$$

$$A = \frac{\delta_C - 2\delta_B}{2\lambda^2}$$

$$y = \left(\frac{\delta_C - 2\delta_B}{2\lambda^2}\right)x^2 + \left(\frac{4\delta_B - \delta_C}{2\lambda}\right)x$$

The slope at $x = 0$

$$\left.\frac{dy}{dx}\right|_{x=0} = \left.\left(\frac{\delta_C - 2\delta_B}{\lambda^2}\right)x + \left(\frac{4\delta_B - \delta_C}{2\lambda}\right)\right|_{x=0} = \frac{4\delta_B - \delta_C}{2\lambda}$$

$$\theta = \frac{4\delta_B - \delta_C}{2\lambda} \quad \ldots\ldots\ldots\ldots\ldots\ldots\ldots\ldots \text{(I)}$$

Appendix F

1. Development of an approximate column equation for axial load only.

From Figs. 6 and 9 ($Rc = 0.3\sigma_y$) the following values of $\frac{Po}{P_y}$ are obtained when $\frac{Mo}{M_y} = 0$.

$\frac{L}{r}$:	0	20	40	60	80	100	120
$\frac{Po}{P_y}$:	1.00	0.96	0.92	0.88	0.83	0.75	0.62

On Fig. 11 this relationship is plotted.

General Equation - assuming a cubic parabola:

$$\frac{Po}{P_y} = a \left(\frac{L}{r}\right)^3 + b \left(\frac{L}{r}\right)^2 + c \left(\frac{L}{r}\right) + d$$

Boundary conditions:

$\frac{L}{r} = 0$ --- $\frac{Po}{P_y} = 1.0$ --- $d = 1.00$

$\frac{L}{r} = 40$ --- $\frac{Po}{P_y} = 0.92$

$\frac{L}{r} = 80$ --- $\frac{Po}{P_y} = 0.83$

$\frac{L}{r} = 120$ --- $\frac{Po}{P_y} = 0.62$

Substituting:

1.) $64{,}000\ a + 1600\ b + 40\ c = -0.08$

2.) $512{,}000\ a + 6400\ b + 80\ c = -0.17$

3.) $1{,}728{,}000\ a + 14{,}400\ b + 120\ c = -0.38$

Solving:

$a = -\frac{1}{3{,}490{,}000}$;

$b = \frac{1}{32{,}000}$;

$c = \frac{-1}{358}$

$$\frac{Po}{P_y} = 1.00 - \frac{1}{3,500,000}\left(\frac{L}{r}\right)^3 + \frac{1}{32,000}\left(\frac{L}{r}\right)^2 - \frac{1}{353}\left(\frac{L}{r}\right) \quad \ldots\ldots\ldots\ldots \text{II}$$

In Table 1 the values of $\frac{Po}{Py}$ are tabulated for L/r. This table is similar to the one furnished by the AISC handbook for allowable column stresses.

Matching only that part of the curve below the Euler value (i.e. $L/r \leq 112$), the simplified expression

$$\frac{Po}{P_y} = 1 - \frac{\left(\frac{L}{r}\right)}{\alpha} - \frac{\left(\frac{L}{r}\right)^2}{\beta}$$ will be obtained

@ $\frac{L}{r} = 50$, $\frac{Po}{P_y} = 0.900$

@ $\frac{L}{r} = 100$, $\frac{Po}{P_y} = 0.755$

$$0.900 = 1 - \frac{50}{\alpha} - \frac{(50)^2}{\beta}$$

$$0.755 = 1 - \frac{100}{\alpha} - \frac{(100)^2}{\beta}$$

Solving for α and β:

$\alpha = 111,000$; $\beta = 645$

then the equation will be:

$$\frac{Po}{P_y} = 1 - \frac{\left(\frac{L}{r}\right)^2}{111,000} - \frac{\left(\frac{L}{r}\right)}{645} \quad \ldots\ldots\ldots\ldots\ldots\ldots \text{IIa}$$

In table 1a the values of Po/P_y are tabulated versus L/r.

TABLE 1

Values of Allowable Axial Thrust (determined from Equation II)

L/r	P_o/P_y	L/r	P_o/P_y	L/r	P_o/P_y
0	1.000	52	0.899	86	0.809
5	0.987	54	0.895	88	0.801
10	0.975	56	0.891	90	0.793
15	0.964	58	0.887	92	0.785
20	0.954	50	0.883	94	0.776
25	0.945	62	0.877	96	0.767
30	0.937	64	0.874	98	0.757
32	0.933	66	0.869	100	0.747
34	0.930	68	0.865	102	0.736
36	0.927	70	0.860	104	0.726
38	0.923	72	0.854	106	0.714
40	0.920	74	0.849	108	0.702
42	0.917	76	0.843	110	0.690
44	0.913	78	0.837	112	0.677
46	0.910	80	0.830	114	0.664
48	0.906	82	0.823	116	0.650
50	0.903	84	0.816	118	0.635
				120	0.620

TABLE 1a

Values of Allowable Axial Thrust (determined from Equation IIa)

L/r	Po/Py	L/r	Po/Py
0	1.000	66	0.858
5	0.992	68	0.853
10	0.984	70	0.847
15	0.975	72	0.842
20	0.965	74	0.836
25	0.956	76	0.830
30	0.945	78	0.824
32	0.941	80	0.818
34	0.937	82	0.812
36	0.933	84	0.806
38	0.928	86	0.800
40	0.924	88	0.794
42	0.919	90	0.787
44	0.914	92	0.781
46	0.910	94	0.775
48	0.905	96	0.768
50	0.899	98	0.761
52	0.895	100	0.755
54	0.890	102	0.748
56	0.885	104	0.741
58	0.880	106	0.755
60	0.875	108	0.728
62	0.869	110	0.720
64	0.864	112	0.713

2. Development of an interaction equation for the condition "c" loading.

Assume the following interaction equation:

$$\frac{Mo}{M_p} = 1.0 - \alpha \frac{Po}{P_y} - \beta\left(\frac{Po}{P_y}\right)^2 \quad \ldots\ldots\ldots\ldots\ldots\ldots \text{(a)}$$

As an example the calculation of α and β will be given for $L/r = 120$.

Note: for all the calculations for this case, $\frac{Po}{P_y} = 0.3$ and $\frac{Po}{P_y} = 0.6$ will be used. (The form of the equation insures $Mo/M_p = 1$ when $\frac{Po}{Py} = 0.$)

1.) $\frac{Po}{Py} = 0.6$; $\frac{Mo}{My} = 0.008$ (from Fig. 6)

2.) $\frac{Po}{Py} = 0.3$ $\frac{Mo}{My} = 0.278$

from Equation a.

$$\alpha + \beta\left(\frac{Po}{P_y}\right) = \frac{1.00 - \frac{Mo}{Mp}}{\frac{Po}{Py}}$$

then

1.) $\alpha + 0.6\,\beta = \frac{1.000 - 0.008}{0.6}$ $\qquad \alpha + 0.6\,\beta = 1.653$

2.) $\alpha + 0.3\,\beta = \frac{1.000 - 0.278}{0.3}$ $\qquad \alpha + 0.3\,\beta = 2.407$

Solving: $\alpha = +3.157$
$\beta = -2.510$

Similarly the values of α and β are computed for the other slenderness ratios.

Following are the computed values of α and β :

L/r	α	β
0	+0.423	+0.770
20	+0.683	+0.500
40	+0.990	+0.167
60	+1.363	-0.217
80	+1.828	-0.753
100	+2.327	-1.313
120	+3.157	-2.510

In Fig. 12 α and β are plotted versus L/r.

The α - curve is approximated by the following cubic equation:

$$\alpha = a_1 + a_2\left(\frac{L}{r}\right) + a_3\left(\frac{L}{r}\right)^2 + a_4\left(\frac{L}{r}\right)^3$$

at $\frac{L}{r} = 0$, $\alpha = 0.420$ $\therefore a_1 = 0.420$

at $\frac{L}{r} = 120$ $\alpha = 3.15$

at $\frac{L}{r} = 80$ $\alpha = 1.80$

at $\frac{L}{r} = 40$ $\alpha = 1.00$

1.) $120\ a_2 + 14{,}400\ a_3 + 1{,}728{,}000\ a_4 = 2.730$

2.) $80\ a_2 + 6400\ a_3 + 512{,}000\ a_4 = 1.380$

3.) $40\ a_2 + 1600\ a_3 + 64{,}000\ a_4 = 0.580$

Solving:

$$a_2 = \frac{1}{68.96};\quad a_3 = \frac{1}{29{,}087};\quad a_4 = \frac{1}{1{,}163{,}700}$$

then $\alpha = 0.420 + \frac{\left(\frac{L}{r}\right)}{69} - \frac{\left(\frac{L}{r}\right)^2}{29,000} - \frac{\left(\frac{L}{r}\right)^3}{1,164,000}$ . . . . . b

The values of α from equation b are plotted in dotted line on Fig. 12. Good correspondence exists.

The β-curve is approximated by the following cubic equation:

$$\beta = 0.770 + b_2\left(\frac{L}{r}\right) + b_3\left(\frac{L}{r}\right)^2 + b_4\left(\frac{L}{r}\right)^3$$

at $\frac{L}{r} = 120$ $\quad \beta = -2.510$

at $\frac{L}{r} = 80$ $\quad \beta = -0.720$

at $\frac{L}{r} = 40$ $\quad \beta = +0.160$

1.) $120b_2 + 14,400\, b_3 + 1,728,000\, b_4 = -3.280$

2.) $80\, b_2 + 6400\, b_3 + 512,000\, b_4 = -1.490$

3.) $40\, b_2 + 1600\, b_3 + 64,000\, b_4 = -0.610$

Solving:

$$b_2 = -\frac{1}{58.095}; \quad b_3 = \frac{1}{8695}; \quad b_4 = -\frac{1}{606,060}$$

$$\beta = 0.770 - \frac{\frac{L}{r}}{58.1} + \frac{\left(\frac{L}{r}\right)^2}{8700} - \frac{\left(\frac{L}{r}\right)^3}{606,000} \quad . . . . . (c)$$

The values of β from Equation (c) are plotted on Fig. 12 in dotted line.

Table 2 contains the values of α and β for various slenderness ratios, determined from Equations (b) and (c).

TABLE 2

Values of α and β for $\frac{Mo}{Mp} = 1.0 - \alpha\frac{Po}{Py} - \beta\left(\frac{Po}{Py}\right)^2$ (Loading condition "c")

L/r	α	β	L/r	α	β
0	0.42	0.77	62	1.39	-0.25
5	0.49	0.69	64	1.43	-0.29
10	0.56	0.61	66	1.47	-0.34
15	0.63	0.53	68	1.52	-0.39
20	0.70	0.46	70	1.56	-0.44
25	0.77	0.39	72	1.61	-0.49
30	0.85	0.31	74	1.65	-0.54
32	0.88	0.28	76	1.70	-0.60
34	0.91	0.25	78	1.75	-0.66
36	0.94	0.22	80	1.83	-0.75
38	0.97	0.19	82	1.85	-0.78
40	0.99	0.17	84	1.90	-0.84
42	1.03	0.13	86	1.96	-0.91
44	1.06	0.10	88	2.01	-0.98
46	1.09	0.06	90	2.07	-1.05
48	1.13	0.03	92	2.13	-1.13
50	1.17	-0.01	94	2.19	-1.20
52	1.20	-0.05	96	2.25	-1.28
54	1.24	-0.08	98	2.32	-1.37
56	1.28	-0.12	100	2.38	-1.45
58	1.31	-0.16	102	2.45	-1.54
60	1.35	-0.21	104	2.52	-1.63

Continuation Table 2

L/r	α	β	L/r	α	β
106	2.59	-1.73	114	2.90	-2.14
108	2.67	-1.83	116	2.98	-2.26
110	2.74	-1.93	118	3.06	-2.37
112	2.82	-2.03	120	3.16	-2.51

3. Development of an interaction equation for the condition "d" loading.

Assume the interaction curve to be the following straight line:

$$\frac{Mo}{Mp} = \alpha\left(\frac{Po}{Py}\right) + \beta \qquad \ldots\ldots\ldots\ldots\ldots\ldots\ldots\ldots (d)$$

For L/r = 120, from Fig. 9:

$\frac{Po}{Py} = 0.50$ ——— $\frac{Mo}{My} = 0$

$\frac{Po}{Py} = 0.10$ $\frac{Mo}{My} = 1.0$

} Determined by drawing the best straight line through the curve in question (by "eye")

1.) $0 = 0.50\alpha + \beta$

2.) $1.0 = 0.10\alpha + \beta$

$\alpha = -2.500$

$\beta = +1.250$

Summary of constants obtained:

L/r :	0	60	80	100	120
α :	-1.111	-1.317	-1.538	-1.887	-2.500
β :	+1.133	+1.172	+1.200	+1.208	+1.250

These values of α and β are plotted versus $\frac{L}{r}$ in Fig. 13.

Assuming for β that $\beta = A + B\left(\frac{L}{r}\right) + C\left(\frac{L}{r}\right)^2$,

$A = 1.133$, since @ $\frac{L}{r} = 0$ $\beta = 1.133$.

When $\frac{L}{r} = 60$, $\beta = 1.172$, and

when $\frac{L}{r}$, $\beta = 1.250$

Therefore

1.) $0.039 = 60\ B + 3600\ C$

2.) $0.117 = 120\ B + 14{,}400\ C$

$$C = \frac{1}{185{,}000}\ ; \qquad B = \frac{1}{3080}$$

or

$$\beta = 1.133 + \frac{1}{3080}\left(\frac{L}{r}\right) + \frac{1}{185{,}000}\left(\frac{L}{r}\right)^2 \quad \ldots\ldots\ldots\ldots \quad (e)$$

The curve represented by this equation is plotted as a dotted line in Fig. 13.

For α assume that

$$\alpha = A + B\left(\frac{L}{r}\right) + C\left(\frac{L}{r}\right)^2 + D\left(\frac{L}{r}\right)^3$$

The matching conditions are chosen as

when $\frac{L}{r} = 0$; $\alpha = -1.11 \longrightarrow A = -1.110$

when $\frac{L}{r} = 60$; $\alpha = -1.32$

when $\frac{L}{r} = 100$; $\alpha = -1.89$

when $\frac{L}{r} = 120$; $\alpha = -2.50$

1.) $60\ B + 3600\ C + 216{,}000\ D = -0.210$

2.) $100\ B + 10{,}000\ C + 1{,}000{,}000\ D = -0.780$

3.) $120\ B + 14{,}400\ C + 1{,}728{,}000\ D = -1.390$

$$B = -\frac{1}{189}; \qquad C = \frac{1}{8{,}889}\ ; \qquad D = -\frac{1}{720{,}000}$$

$$\alpha = -1.110 - \frac{\left(\frac{L}{r}\right)}{189} + \frac{\left(\frac{L}{r}\right)^2}{8,889} - \frac{\left(\frac{L}{r}\right)^3}{720,000} \quad \ldots\ldots\ldots\ldots\ldots\ldots \text{(f)}$$

The curve representing this equation is plotted as a dotted line in Fig. 14. Good agreement is noted for both α and β with the original curves.

Table 3 contains values of α and β determined from Equations (e) and (f). Intermediate values may be interpolated.

Table 3

Values of α and β for $\frac{Mo}{Mp} = \alpha \frac{Po}{Py} + \beta$

(Loading Condition "d")

L/r	α	β
5	-1.134	1.135
10	-1.153	1.137
15	-1.169	1.139
20	-1.182	1.142
25	-1.194	1.144
30	-1.205	1.148
35	-1.217	1.151
40	-1.231	1.155
45	-1.247	1.159
50	-1.267	1.163
55	-1.292	1.167
60	-1.323	1.172
65	-1.360	1.177
70	-1.406	1.182
75	-1.460	1.188
80	-1.524	1.194
85	-1.600	1.200
90	-1.688	1.206
95	-1.788	1.213
100	-1.903	1.220
105	-2.033	1.227
110	-2.179	1.234
115	-2.343	1.242
120	-2.525	1.250

Appendix G

Table 4

Test results of Johnston and Cheney

Test No.	Member	Material	Eccentricity inches	L/r_x	P max kips	Po/P_y
C-49	I	1	1.01"	22.6	38.6	0.555
C-50	I	1	1.01	32.6	37.5	0.540
C-51	I	2	1.01	42.1	33.5	0.501
C-52	I	2	1.01	47.1	31.3	0.468
C-53	I	2	1.01	52.1	32.8	0.490
C-54	I	2	1.01	62.0	30.7	0.458
C-55	I	2	1.01	72.0	27.0	0.405
C-56	I	2	1.01	82.0	24.5	0.366
C-57	I	2	1.01	101.8	18.7	0.280
C-58	I	2	1.01	121.6	15.6	0.233
C-59	I	2	0.50	22.3	47.4	0.709
C-60	I	2	1.52	22.3	31.2	0.466
C-61	I	2	2.02	22.3	25.6	0.383
C-62	I	2	3.03	22.3	19.4	0.291
C-63	I	2	5.05	22.3	13.9	0.207
C-64	I	2	7.07	22.3	10.3	0.154
C-65	I	2	0.50	47.1	44.6	0.667
C-66	I	2	1.52	47.1	26.8	0.401
C-67	I	2	2.02	47.1	21.8	0.326
C-68	I	2	3.03	47.1	18.2	0.272

Continuation of Table 4

Test No.	Member	Material	Eccentricity inches	L/r_x	P max kips	Po/P_y
C-69	I	2	5.05	47.1	12.2	0.182
C-70	I	2	7.07	47.1	9.2	0.138
C-71	I	2	0.50	72.0	34.6	0.516
C-72	I	2	1.52	72.0	22.8	0.342
C-73	I	2	2.02	72.0	20.8	0.311
C-74	I	2	3.03	72.0	14.8	0.221
C-75	I	2	5.05	72.0	10.7	0.160
C-76	I	2	7.07	72.0	7.9	0.118
6-5	II	3	2.23	46.7	127.6	0.543
6-6	II	3	4.45	46.9	85.0	0.363

Material and Section Properties of the Test Sections of Johnston and Cheney's Experiments:

1.) Member I

Section: 315.7

Area: 1.64 in^2

Depth: 3.00 in

I_{xx}: 2.5 in^4

S_{xx}: 1.7 in^3

r_{xx}: 1.23 in

Plastic Modulus (f): 1.14

Yield strength: Lot 1. σ_y = 42.2 ksi; $M_p = 81.9^{"K}$

Lot 2. σ_y = 40.8 ksi; $M_p = 79.3^{"K}$

2.) Member II

Section: 6 WF 20

Area: 5.90 in^2

Depth: 6.20 in

I_{xx}: 41.7 in^4

S_{xx}: 13.4 in^3

r_{xx}: 2.66 in

Plastic modulus (f): 1.12

Yield strength: Lot 3. σ_y = 39.8 ksi; $M_p = 596^{"K}$

Table 5

Eccentricity Ratios for Johnston and Cheney's Tests

3I5.7

e	$\frac{ec}{r^2}$	$\frac{ec}{r^2}$ (approx.)
0.50"	0.496	1/2
1.01"	1.001	1
1.52"	1.507	1 1/2
2.02"	2.003	2
3.03"	3.004	3
5.05"	5.007	5
7.07"	7.010	7

6 WF 20

e	$\frac{ec}{r^2}$	$\frac{ec}{r^2}$ (approx.)
2.23	0.977	1
4.45	1.949	2

Table 6

Massonnet's Test Results, Loading Case "c"

Test No.	Section	$\frac{ec}{r^2}$	P max (tons)	P_y (tons)	L/r_x	Corrected L/r_x	Po/P_y
1	DIE 20	0.5	88.8	132	23.6	23.2	0.672
2	"	1.0	66.8	132	23.7	23.3	0.506
3	"	3.0	35.8	132	23.7	23.3	0.271
8	"	0.5	84.8	134	35.6	34.9	0.633
9	"	1.0	64.8	133	35.4	34.8	0.487
10	"	3.0	32.8	133	35.5	34.8	0.247
16	"	0.5	71.0	135	44.4	43.5	0.526
17	"	1.0	59.0	134	44.2	43.3	0.440
18	"	3.0	32.5	134	44.4	43.4	0.242
24	"	0.5	62.0	134	59.1	58.0	0.462
25	"	1.0	53.5	133	58.7	57.6	0.402
26	"	3.0	29.0	134	59.2	58.1	0.216
33	DIE 10	0.5	22.8	53.8	80.8	75.0	0.424
34	"	1.0	19.3	54.5	82.4	76.5	0.354
35	"	3.0	11.5	55.0	82.6	76.7	0.209
42	"	0.5	13.8	57.1	109.9	102.0	0.241
43	"	1.0	12.4	55.6	110.3	102.5	0.223
44	"	3.0	9.05	55.7	109.6	101.8	0.163

Table 7

Massonnet's Test Results, Loading Case "d"

Test No.	Section	$\frac{ec}{r^2}$	P max (tons)	P_y (tons)	L/r_x	$L/r_x(33)$	Po/P_y
4	DIE 20	0.5	95.0	133	23.6	23.2	0.715
5	"	1.0	78.8	133	23.6	23.2	0.593
11	"	0.5	93.8	134	35.6	35.0	0.700
12	"	1.0	74.8	133	35.3	34.7	0.562
13	"	3.0	40.3	133	35.2	34.6	0.303
19	"	0.5	90.8	133	47.4	46.5	0.683
20	"	1.0	70.0	133	47.7	46.8	0.526
21	"	3.0	39.0	134	47.7	46.8	0.291
27	"	0.5	82.0	133	59.0	58.0	0.616
28	"	1.0	67.0	135	59.6	58.6	0.496
29	"	3.0	38.1	135	59.2	58.2	0.282
36	DIE 10	0.5	25.0	56.4	81.9	76.0	0.444
37	"	1.0	24.4	56.4	82.7	76.9	0.433
38	"	3.0	15.05	57.0	82.7	76.9	0.264
45	"	0.5	11.8	57.7	109.1	101.5	0.204
47	"	3.0	10.8	57.7	109.1	101.5	0.187

r_x (DIE 20) = 8.24 cm (Handbook value)

r_x (DIE 10) = 3.97 cm (Handbook value)

DIE 10 - σ_y = 26.875 kg/mm^2 = 38.2 ksi; $\sqrt{\frac{33}{38.2}}$ = 0.929 = correction factor

DIE 20- σ_y = 24.056 kg/mm^2 = 34.2 ksi; $\sqrt{\frac{33}{34.2}}$ = 0.982 = correction factor

Table 8
Test Results of the Current Lehigh Test Series

Test No.	Member	Loading Conditions	Experimental* σ_y = 40ksi+ Po/Py	Mo/Py	Adjusted σ_y# Po/Py	Mo/Mp	Adjusted L/r_x	Theoretical Po/Py	Mo/Mp
T-8	8WF31	c	0.62	0.12	0.68	0.13	52	0.76	0.13
T-11	8WF31	c	0.87	0	0.95	0	52	0.90	0
T-12	8WF31	c	0.12	0.84	0.13	0.92	52	0.13	0.86
T-15	8WF31	c	0.85	0	0.93	0	39	0.93	0
T-16	8WF31	c	0.12	0.78	0.13	0.85	39	0.13	0.89
T-18	8WF31	c	0.91	0	0.99	0	25	0.96	0
T-19	8WF31	c	0.12	0.81	0.13	0.88	25	0.13	0.92
T-20	4WF13	c	0.12	0.84	0.12	0.87	50	0.12	0.88
T-26	4WF13	c	0.12	0.79	0.12	0.81	76	0.12	0.82
T-28	4WF13	c	0.80	0	0.82	0	76	0.83	0
T-32	4WF13	c	0.12	0.76	0.12	0.78	101	0.12	0.76
T-13	8WF31	d	0.12	1.05	0.13	1.14	52	0.13	0.95
T-23	4WF13	d	0.12	1.05	0.12	1.08	76	0.12	0.96
T-31	4WF13	d	0.12	0.98	0.12	1.01	101	0.12	0.95

* Parameters that were held constant are underlined.

\+ σ_y= 40 ksi determined from tension coupons

\# Adjusted σ_y is obtained by pro-rating the tension coupon value in the same ratios as those given in Ref. 13.
(Note: values change for different sections.)

Table 9

Wisconsin Test Results

Test No.	ec/r^2	L/r_x	L/r_x (33)	σ_y	$\sigma_{ult.}$ (ksi)	Po/Py
H-1	1.00	11.4	10.7	37.4 ksi	20.7	0.553
H-2	1.00	29.0	27.2	37.4	19.95	0.533
H-3	1.00	49.5	46.5	37.4	17.95	0.480
H-4	1.00	69.6	65.0	38.0	15.10	0.398
H-5	1.00	89.7	35.4	36.4	12.60	0.346

F I G U R E S

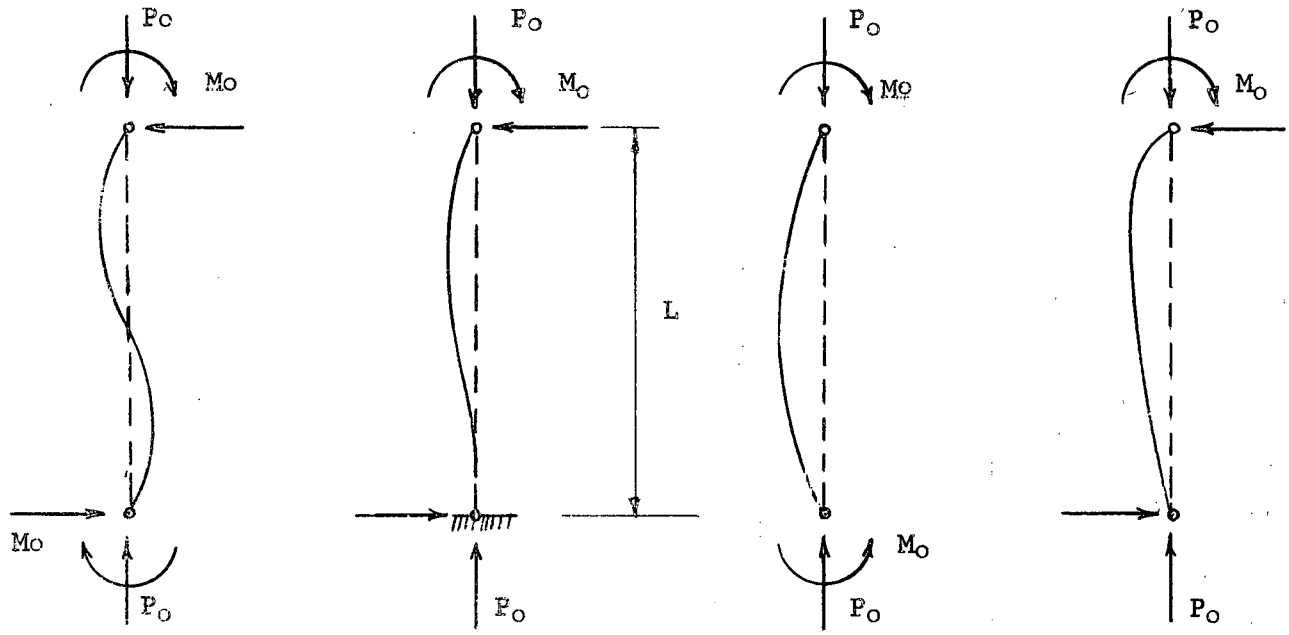

Figure 1

Basic Conditions of Loading

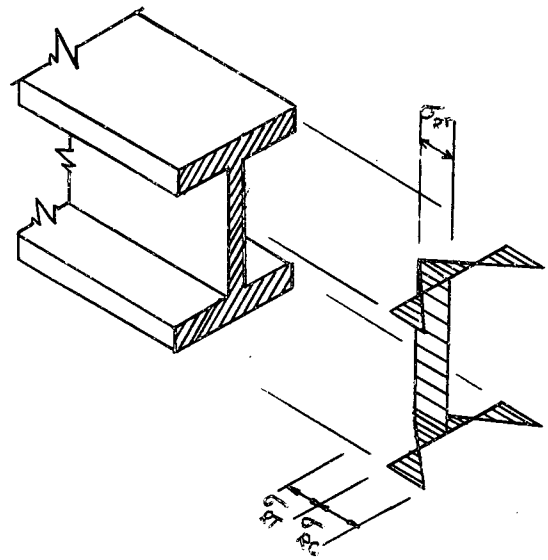

$$\sigma_{RC} = 0.3\sigma_y$$

$$\sigma_{RT} = \left[\frac{bt}{bt+w(d-2t)}\right] \sigma_{RC}$$

Figure 2

Assumed Cooling Residual Stress Pattern

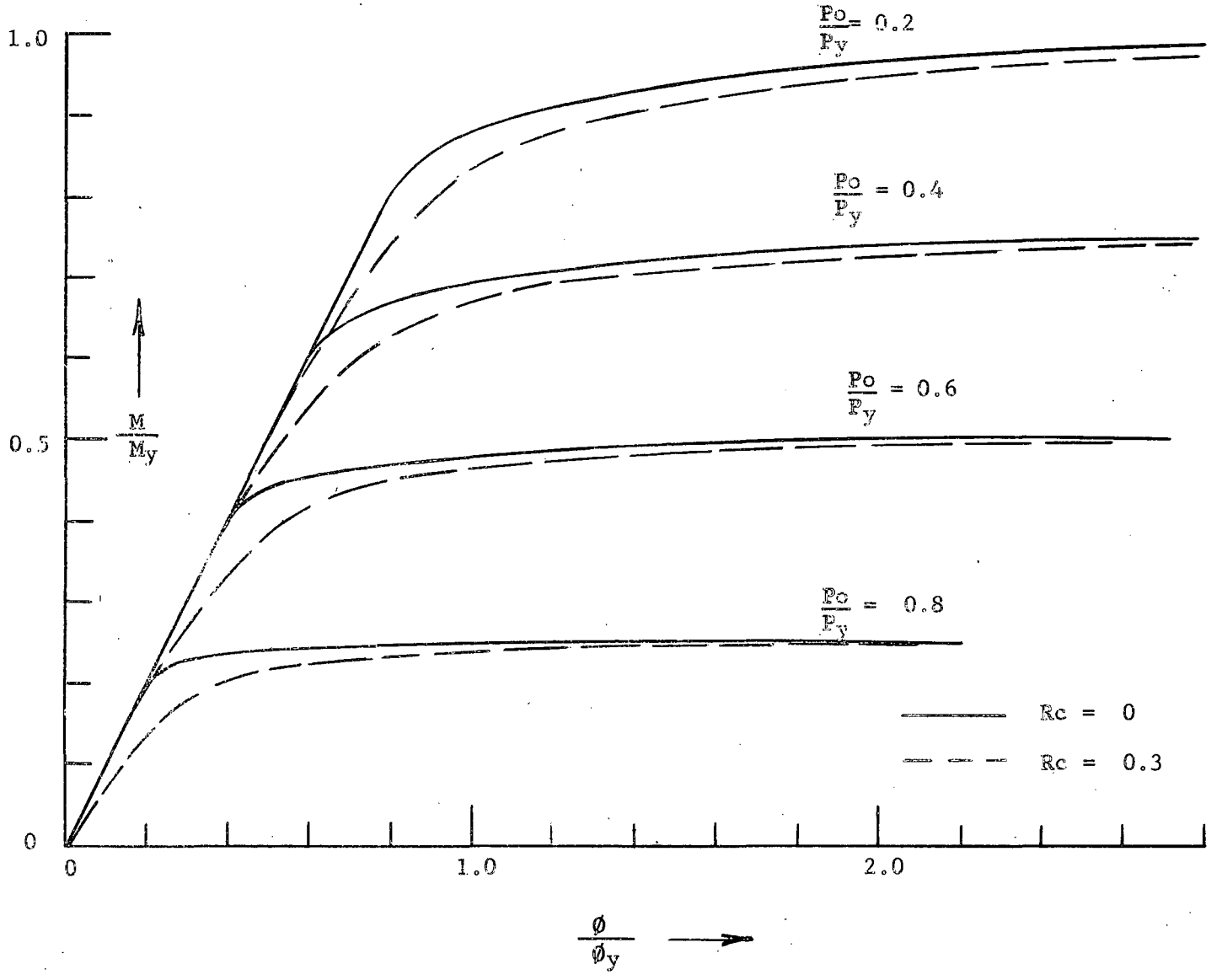

Figure 3

Moment-Thrust-Curvature Relationships for an 8WF 31 Section, Including the Influence of Residual Stress

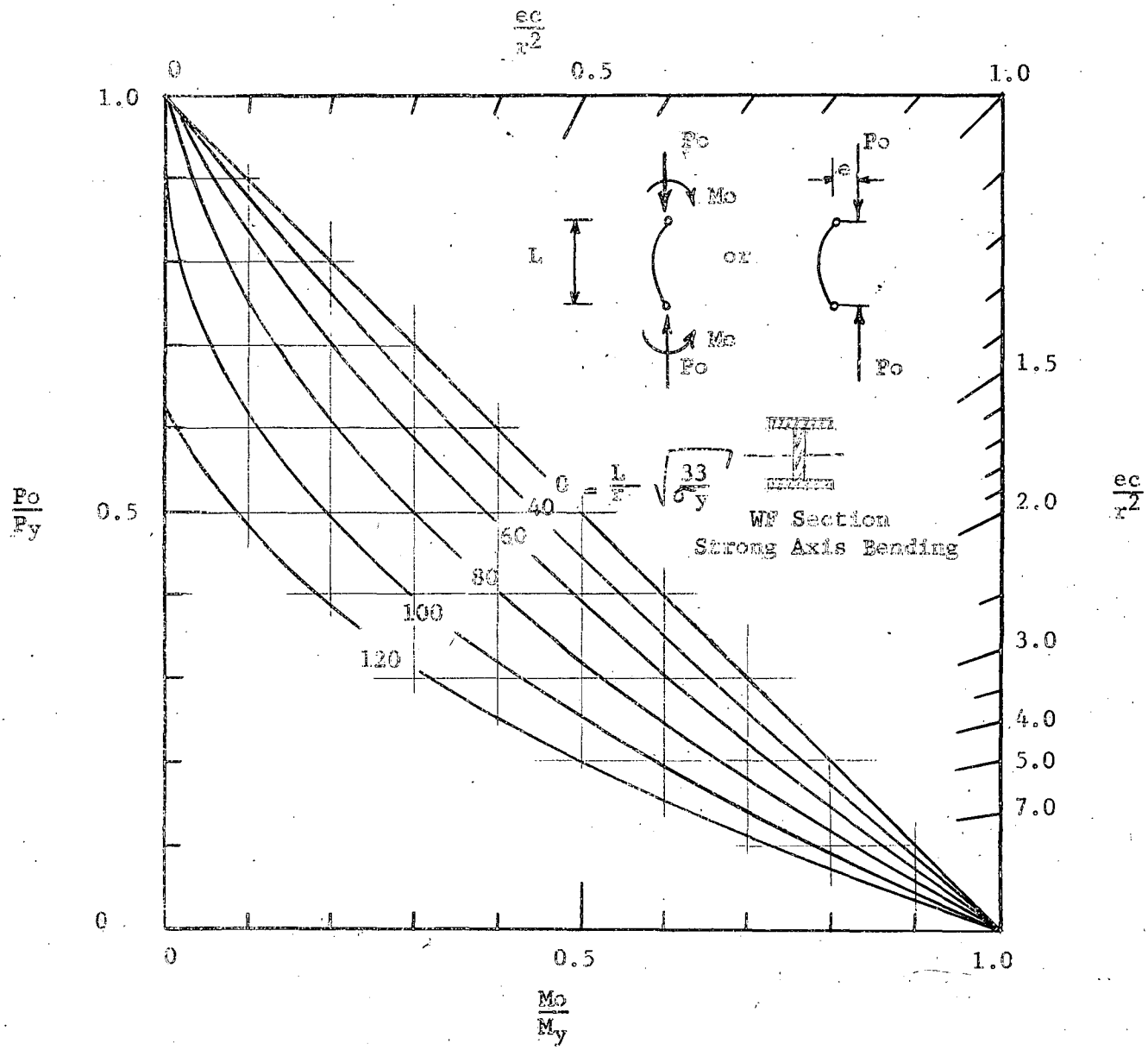

Note: σ_y = Yield Stress in ksi

Figure 4

Initial Yield Interaction Curves for Condition "c" Loading

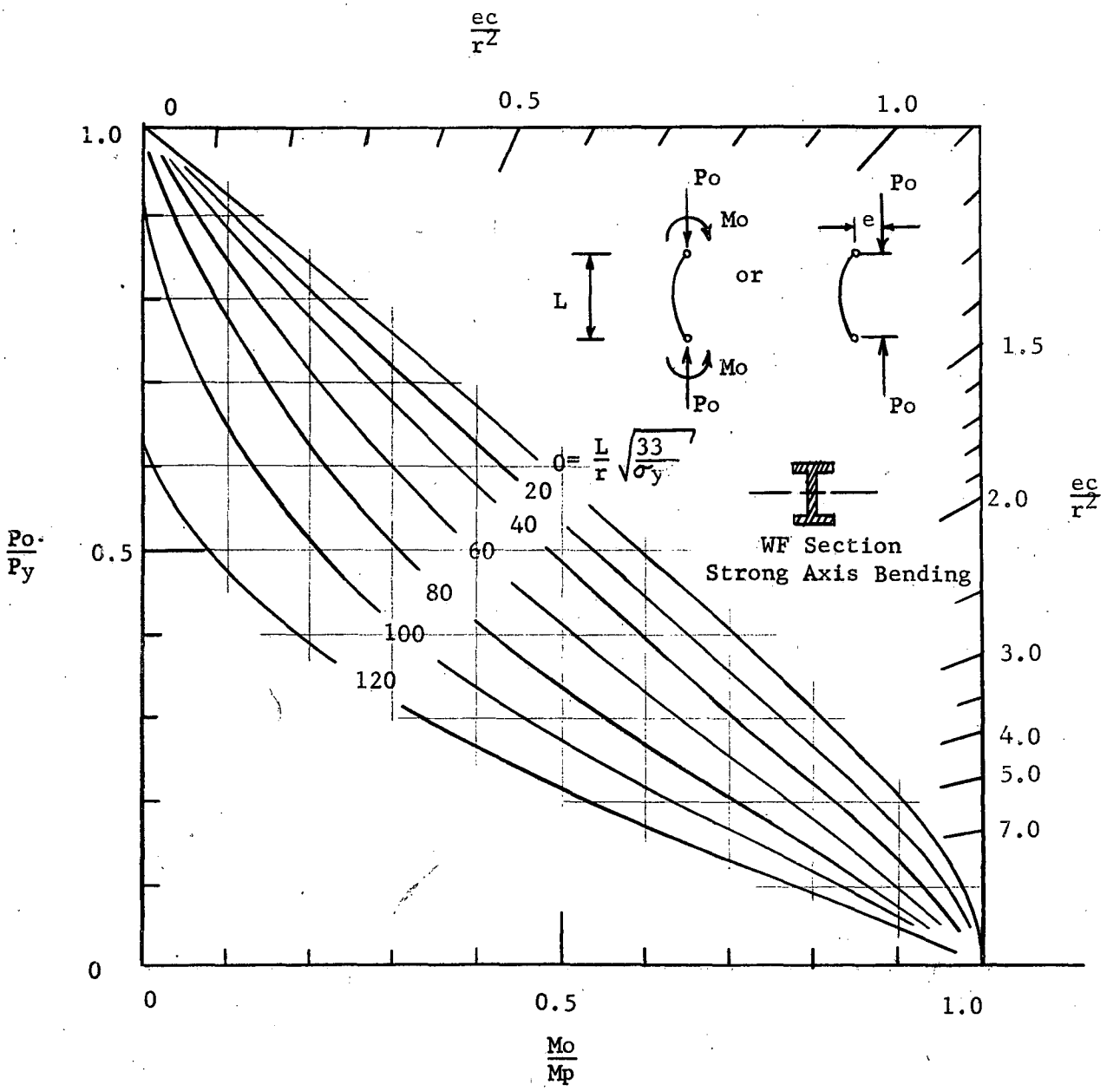

Note: σ_y = Yield Stress in ksi

Figure 5

Maximum Strength Interaction Curves for Condition "c" Loading, Neglecting Residual Stress.

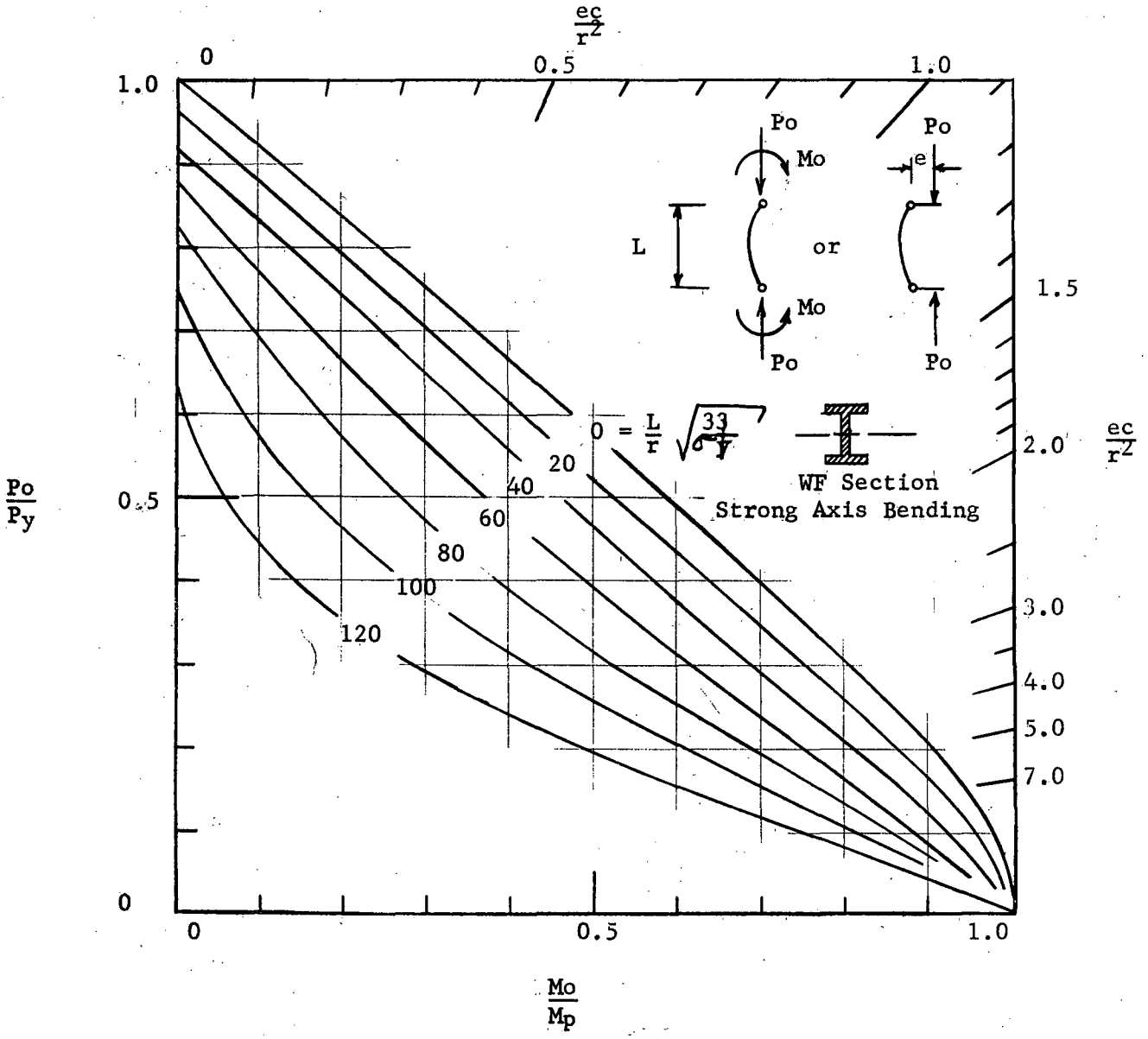

Note: σ_y = Yield stress in ksi

Figure 6

Maximum Strength Interaction Curves for Condition "c" Loading, Including Influence of Residual Stress ($\sigma_{RC} = 0.3\ \sigma_y$)

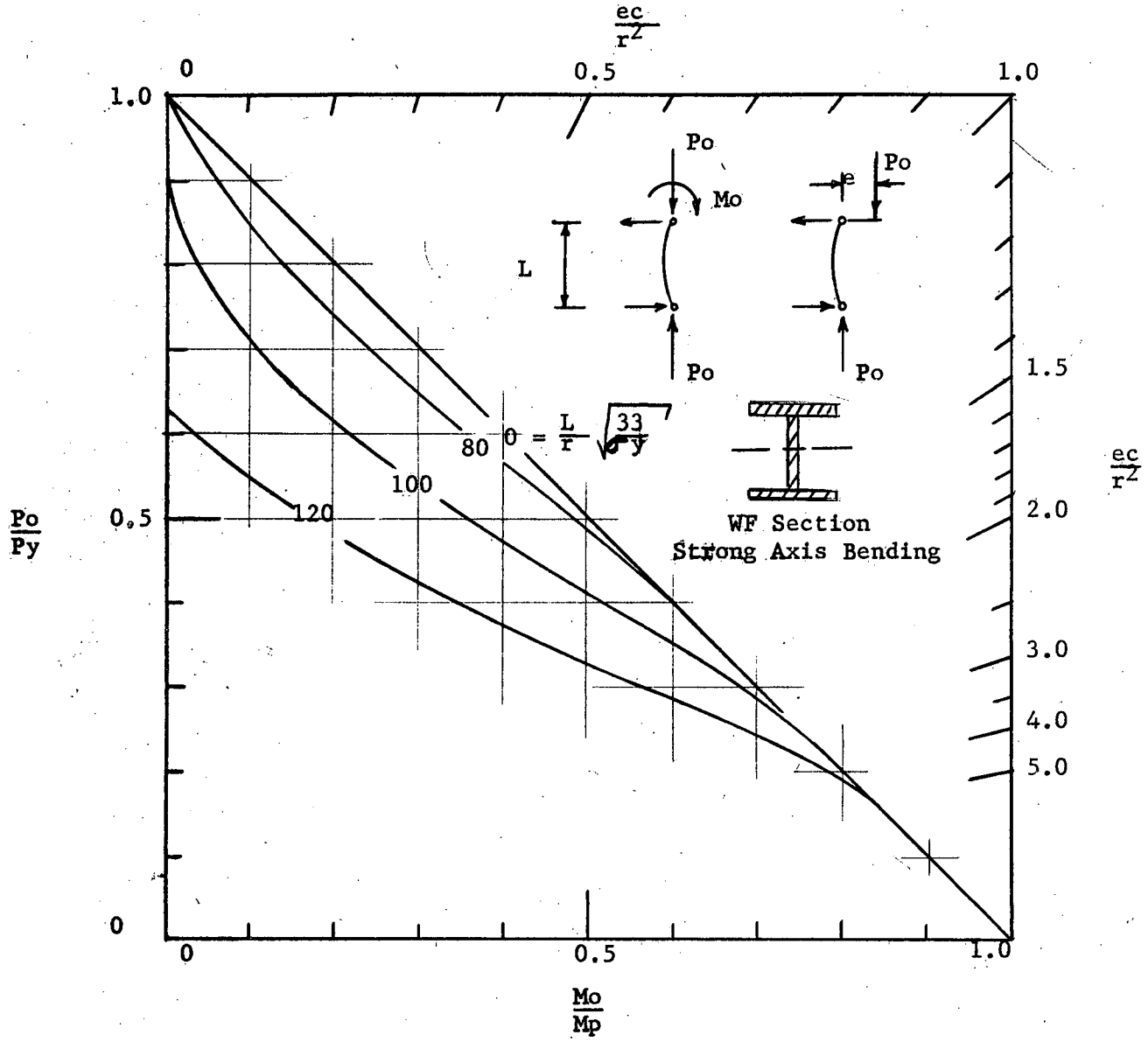

Note: σ_y = Yield Strength in ksi

Figure 7

Initial Yield Interaction Curves for Condition "d" Loading

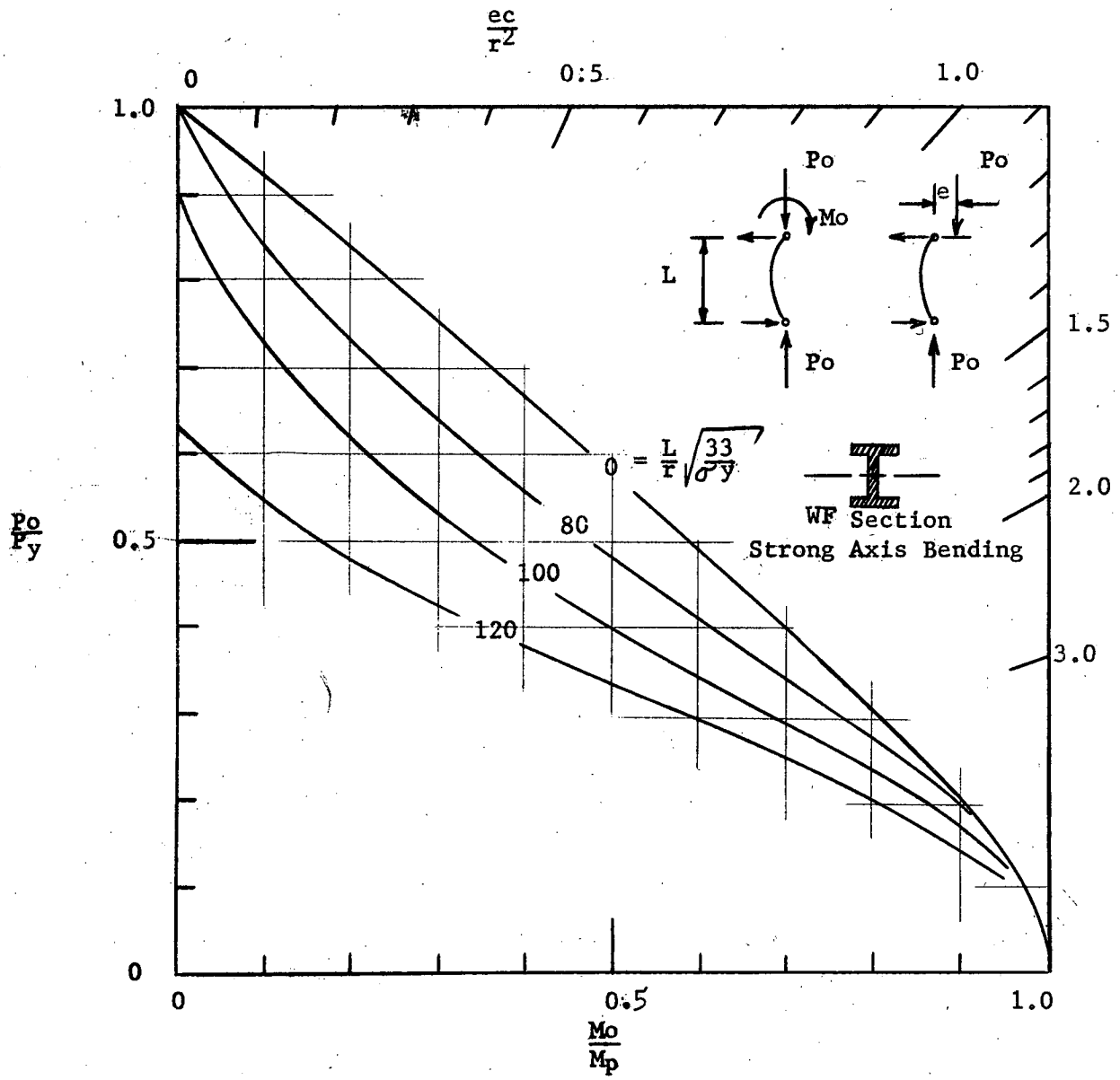

Note: σ_y = Yield stress in ksi

Figure 8

Maximum Strength Interaction Curves for Condition "d" Loading, Neglecting Residual Stress

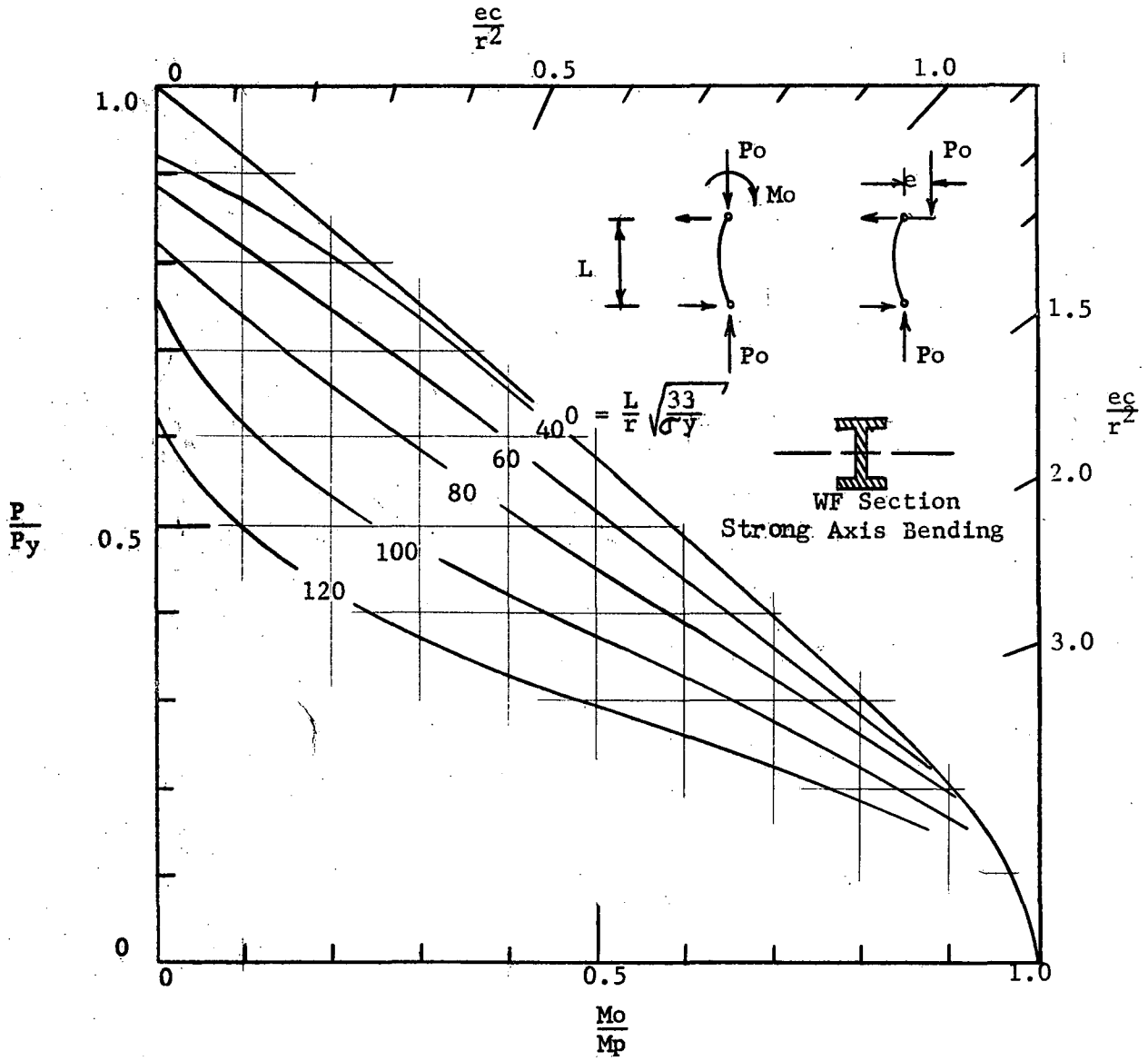

Note: σ_y = Yield Stress in ksi

Figure 9

Maximum Strength Interaction Curves for Condition "d" Loading, Including the Influence of Residual Stress (Rc = 0.3)

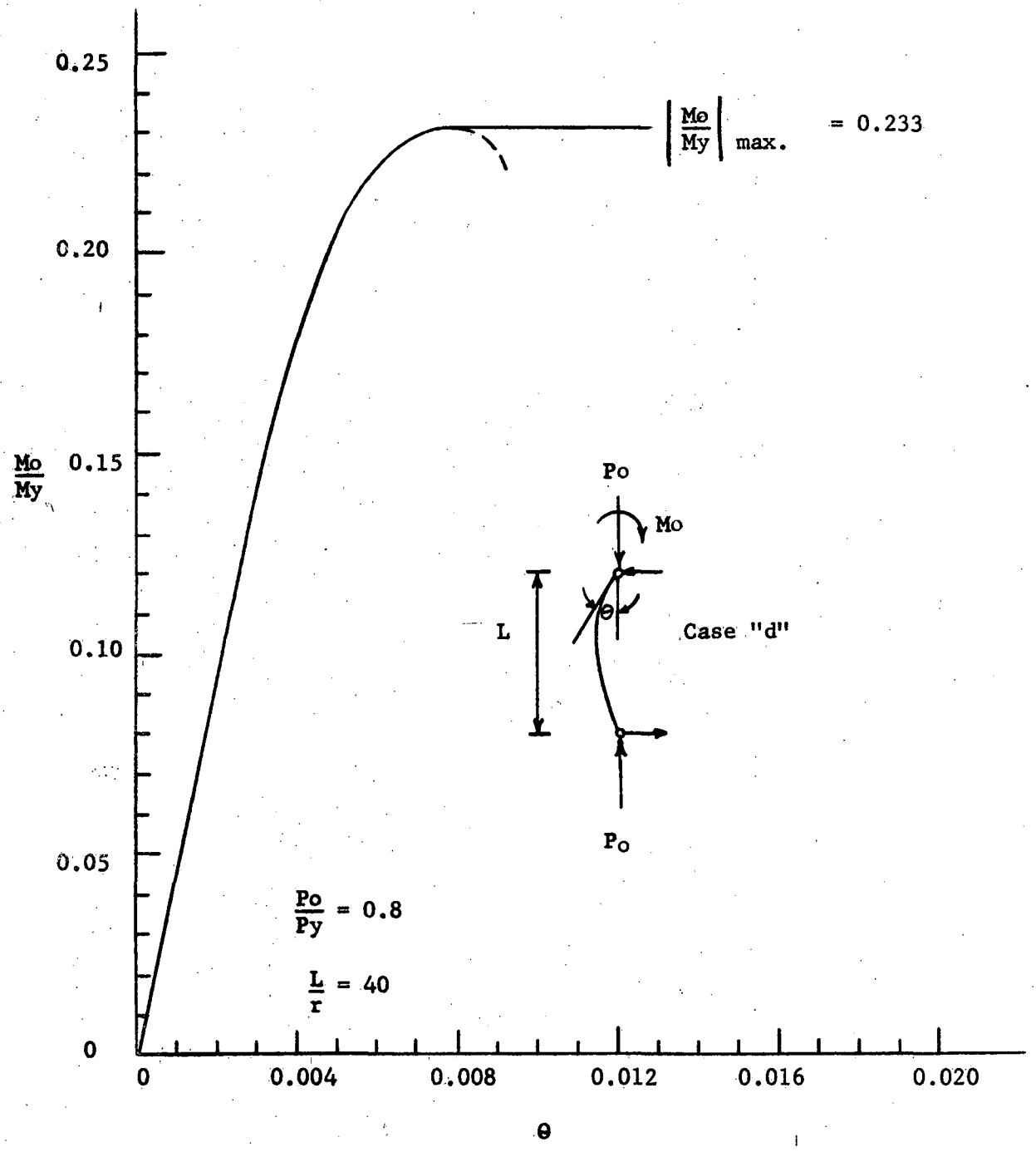

Figure 10

Typical Moment vs. End-Rotation Curve for Condition "d" Loading

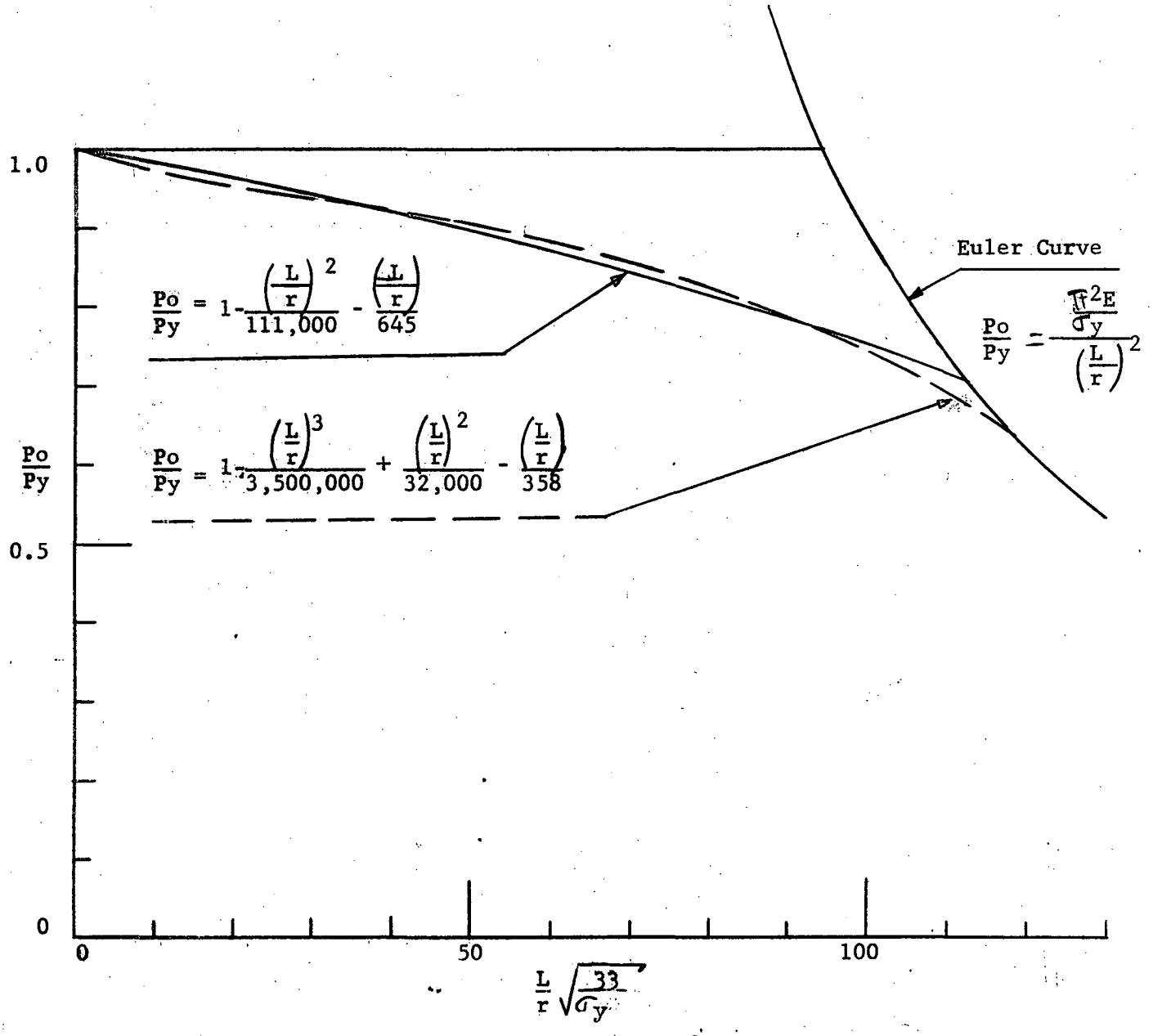

Note: σ_y = Yield Stress in ksi

Figure 11

Approximate Equation for Axial Load Only (Rc = $0.3\sigma_y$)
(Column Pinned in Strong Direction and Fixed in Weak Direction)

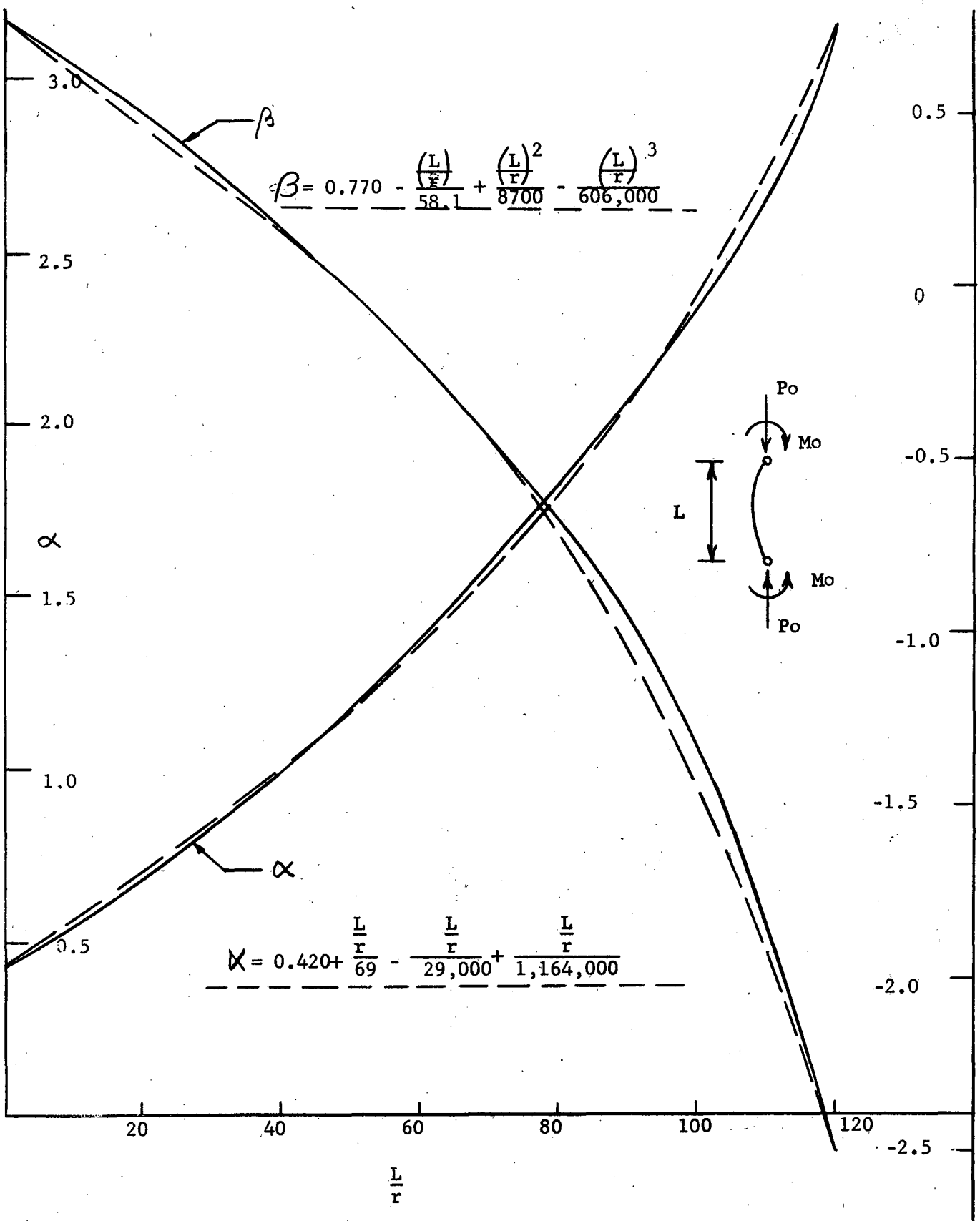

Figure 12

Coefficients α and β for Condition "c" Interaction Curves

$$\frac{Mo}{Mp} = 1.0 - \left(\frac{P}{Py}\right)\left[\alpha + \beta\left(\frac{Po}{Py}\right)\right] \quad \ldots\ldots\ldots\ldots (8)$$

where

$$\alpha = 0.420 + \frac{\left(\frac{L}{r}\right)}{69} - \frac{\left(\frac{L}{r}\right)^2}{29{,}000} + \frac{\left(\frac{L}{r}\right)^3}{1{,}164{,}000}$$

$$\beta = 0.770 \frac{\left(\frac{L}{r}\right)}{58.1} + \frac{\left(\frac{L}{r}\right)^2}{8{,}700} - \frac{\left(\frac{L}{r}\right)^3}{606{,}000} \quad \ldots\ldots (8b)$$

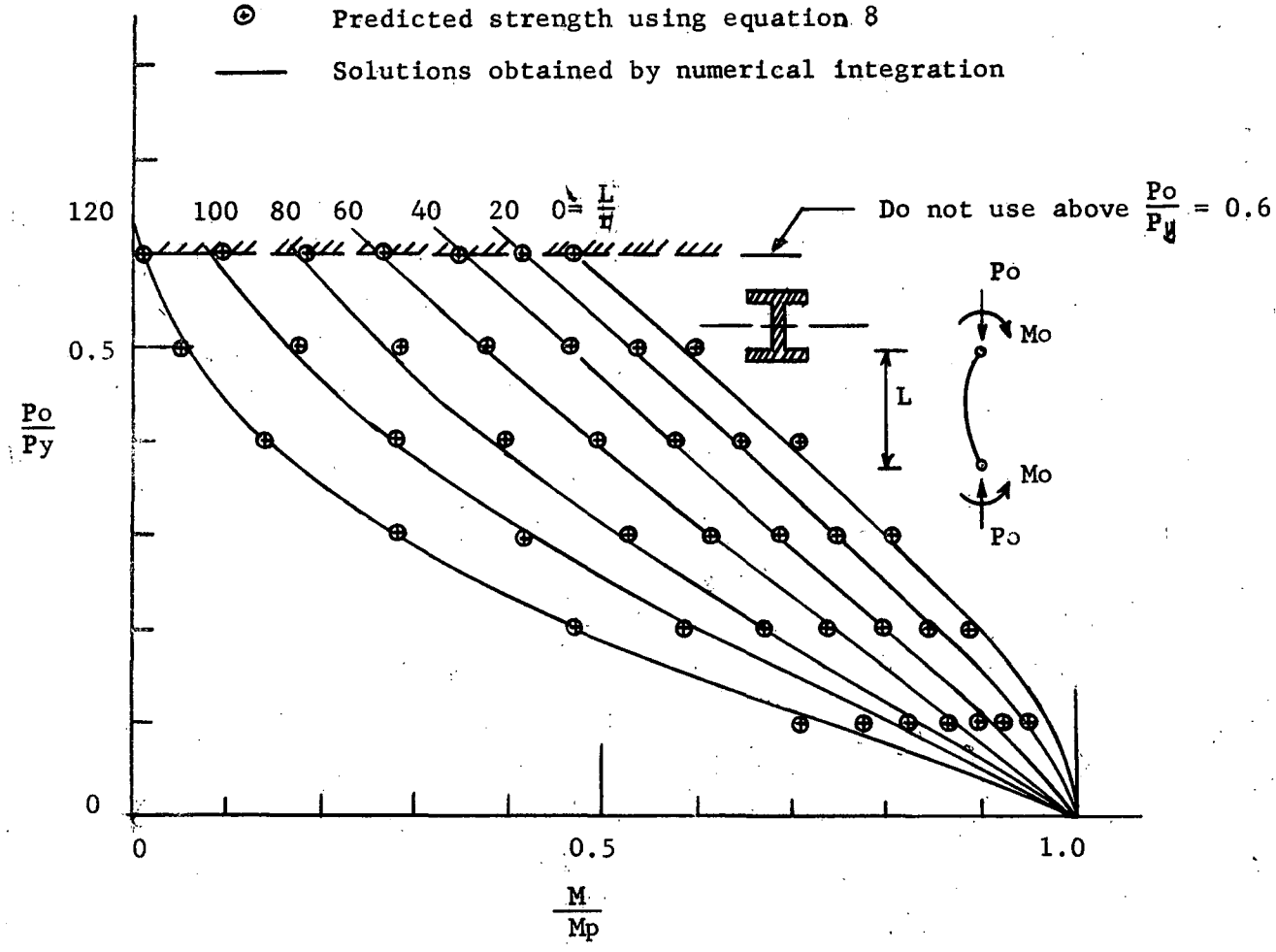

Figure 13

Comparison between "Exact" and "Approximate" Interaction Curve, for Loading Condition "C".

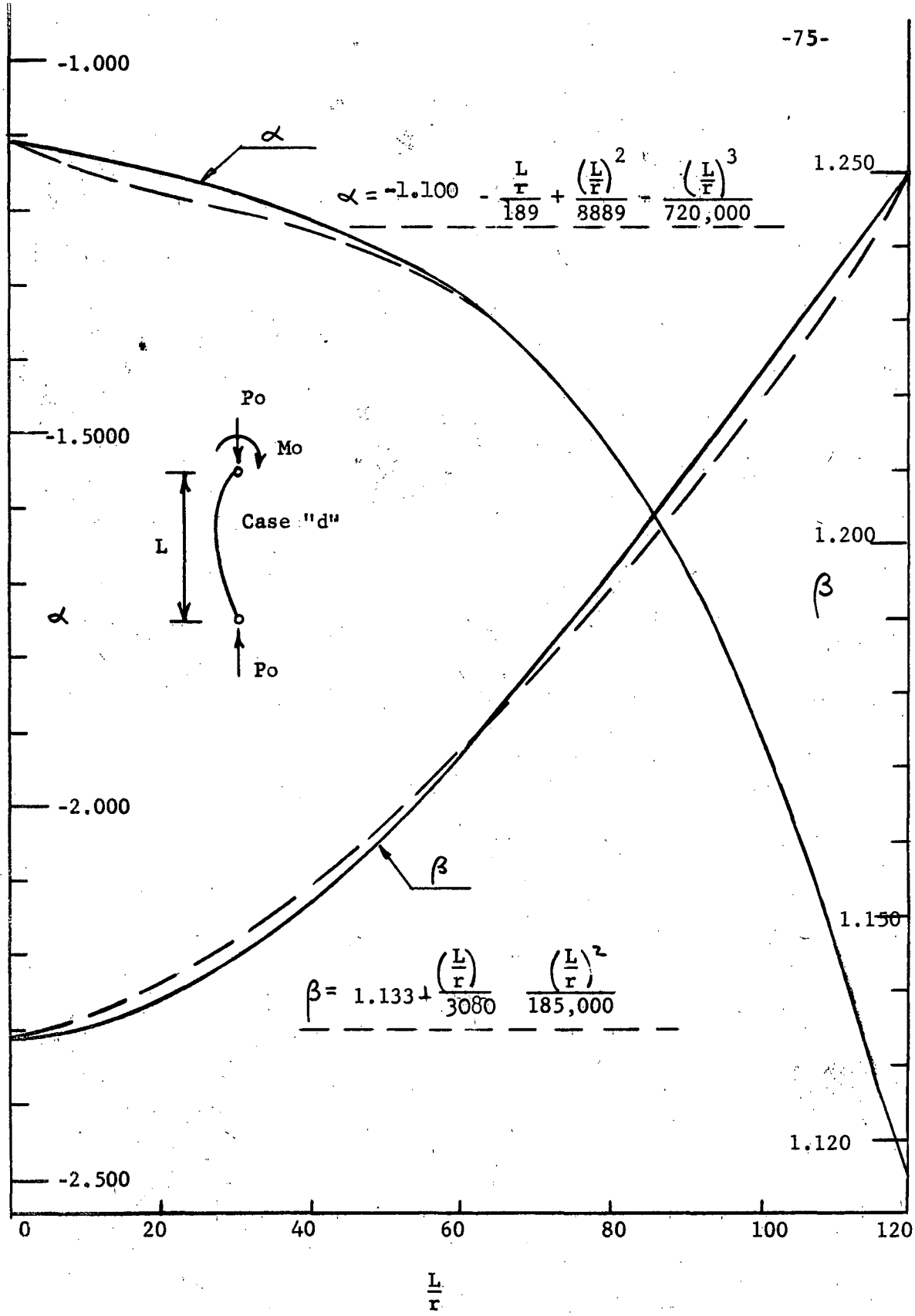

Figure 14

Coefficients α and β for Condition "d" Interaction Curves

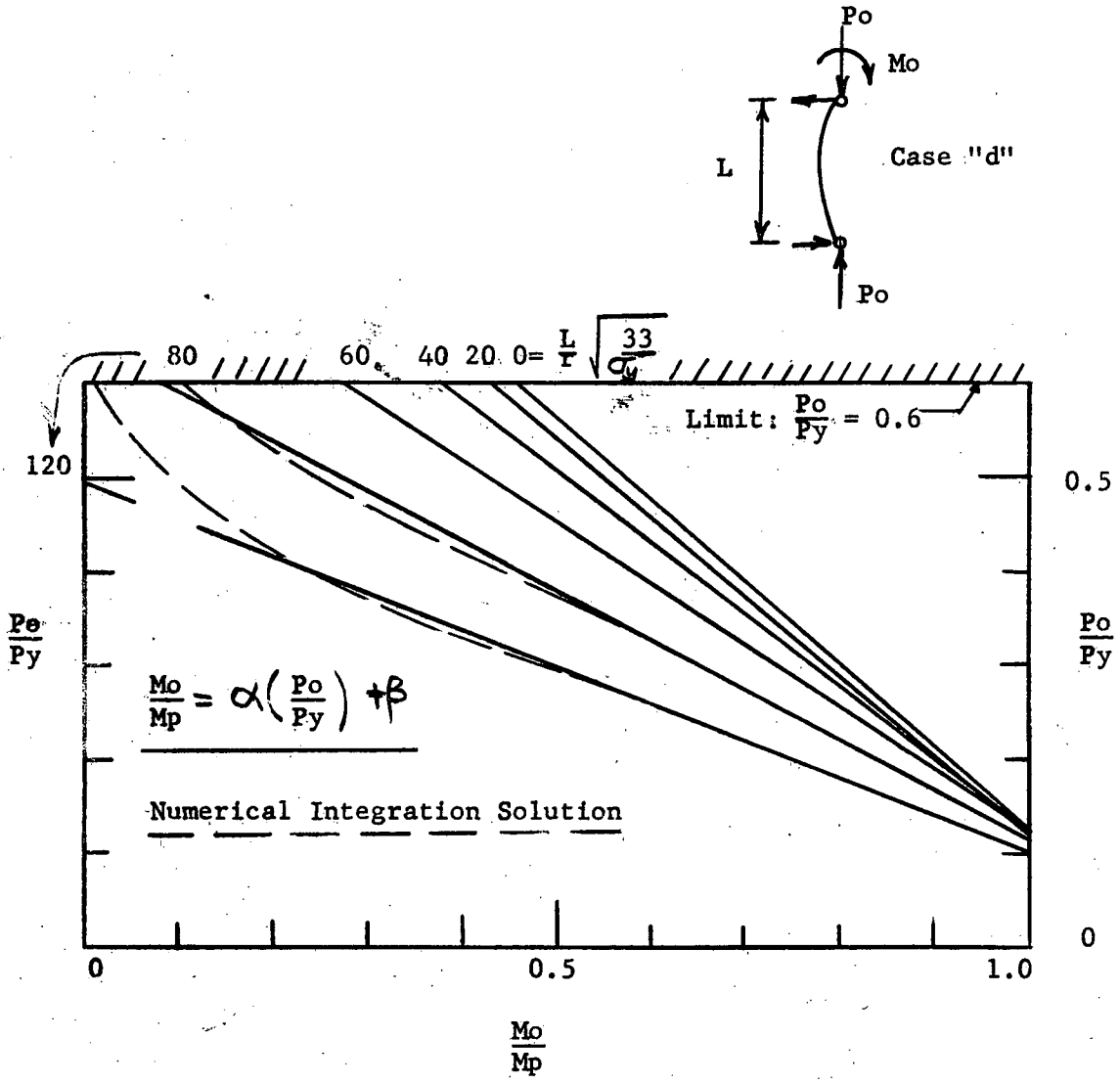

Figure 15

Comparison between "Exact" and "Approximate" Interaction Curve, for Condition "d" Loading.

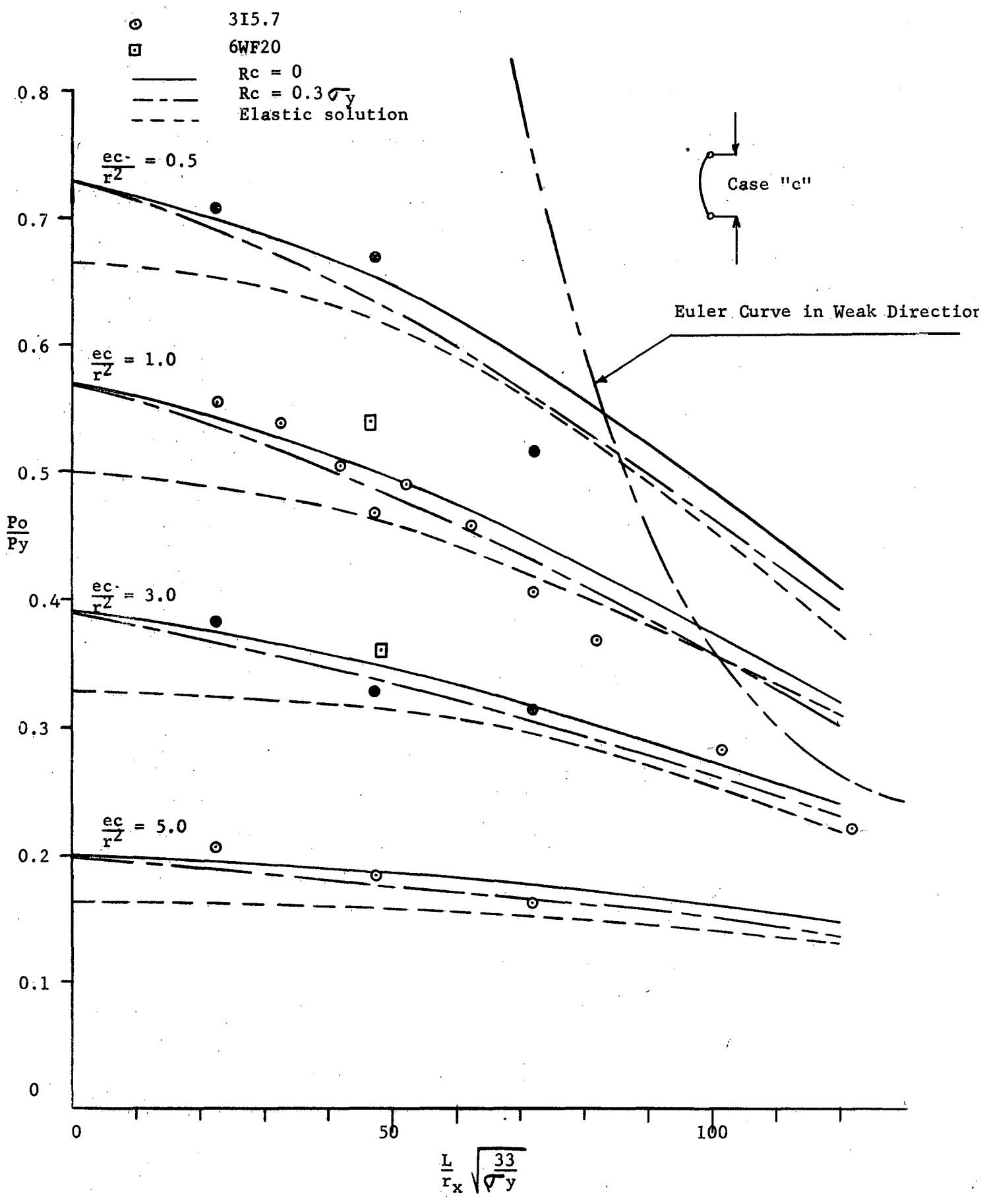

Figure 16

Comparison with Test Results of Johnston and Cheney

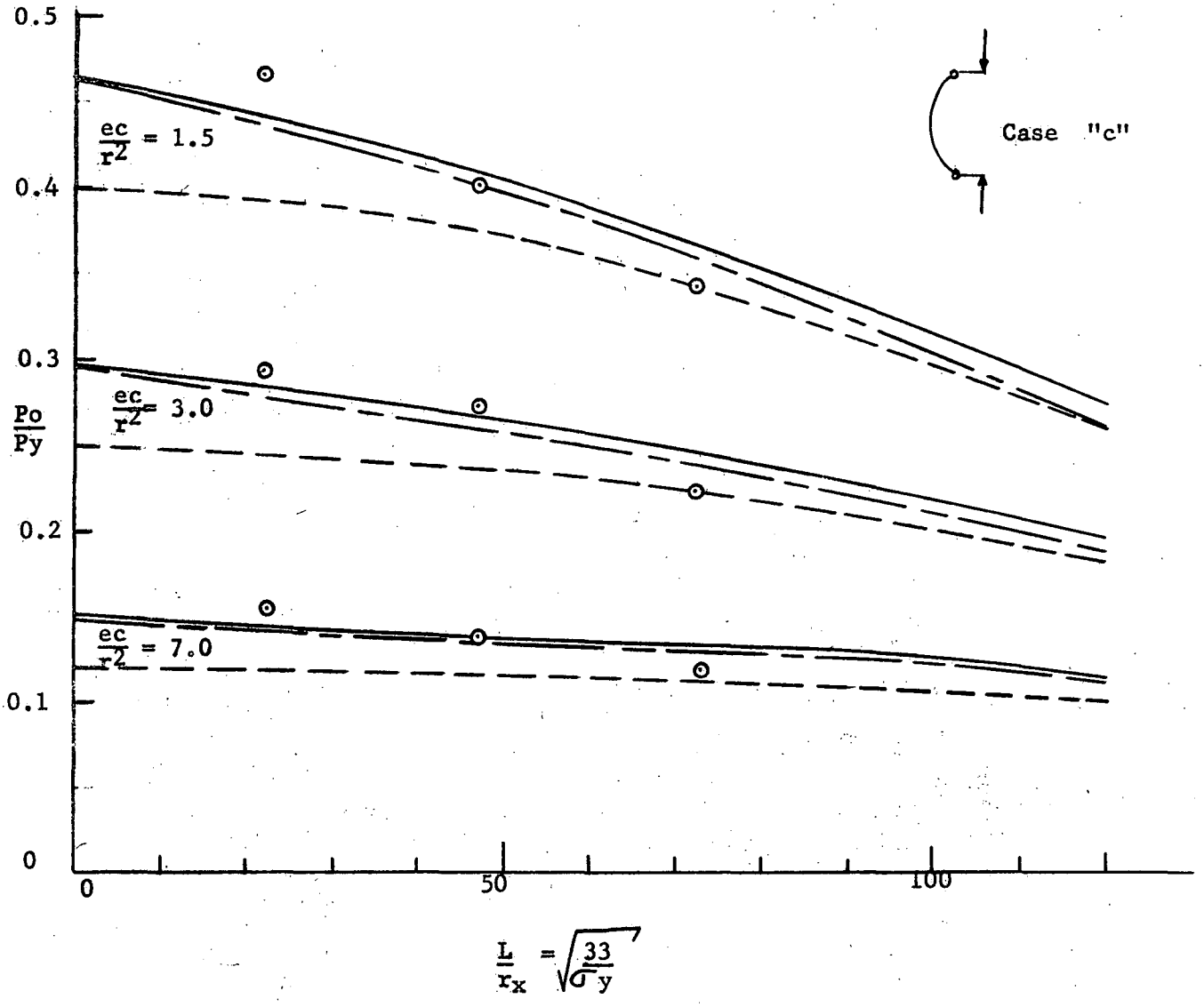

Figure 17

Comparison with Test Results of Johnston and Cheney
(Continuation of Figure 16)

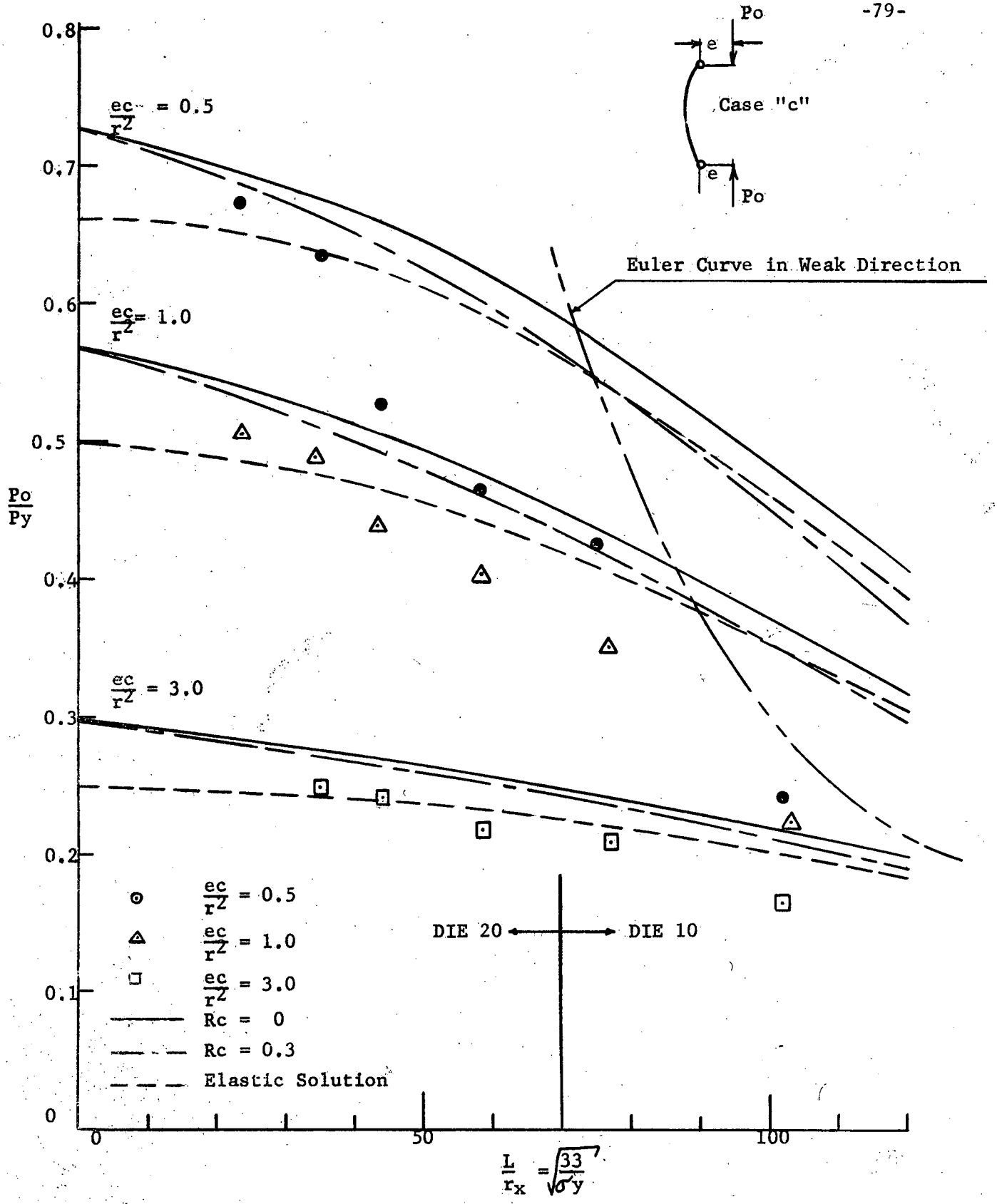

Figure 18

Comparison with Test Results of Massonnet

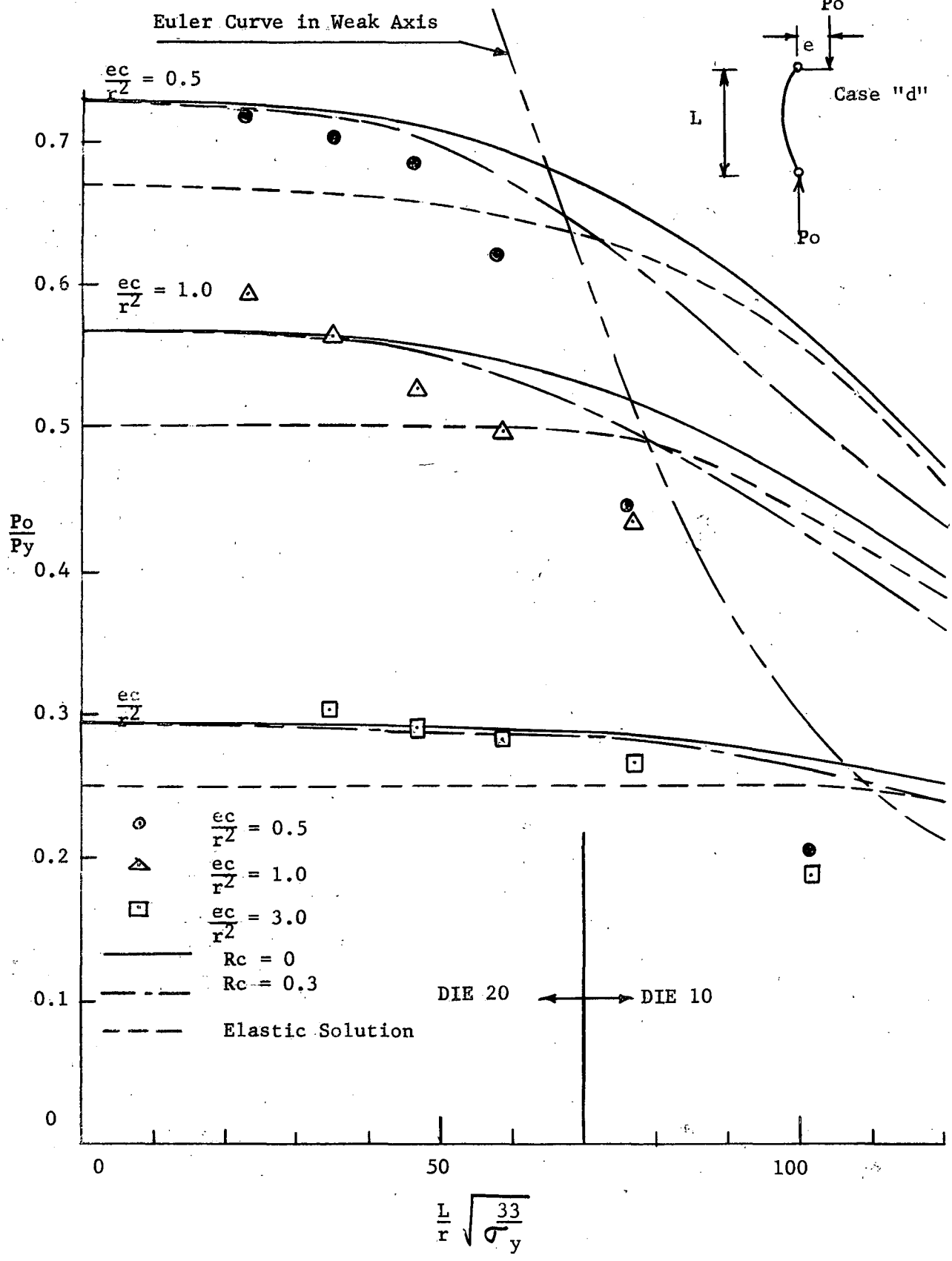

Figure 19

Comparison with Test Results of Massonnet

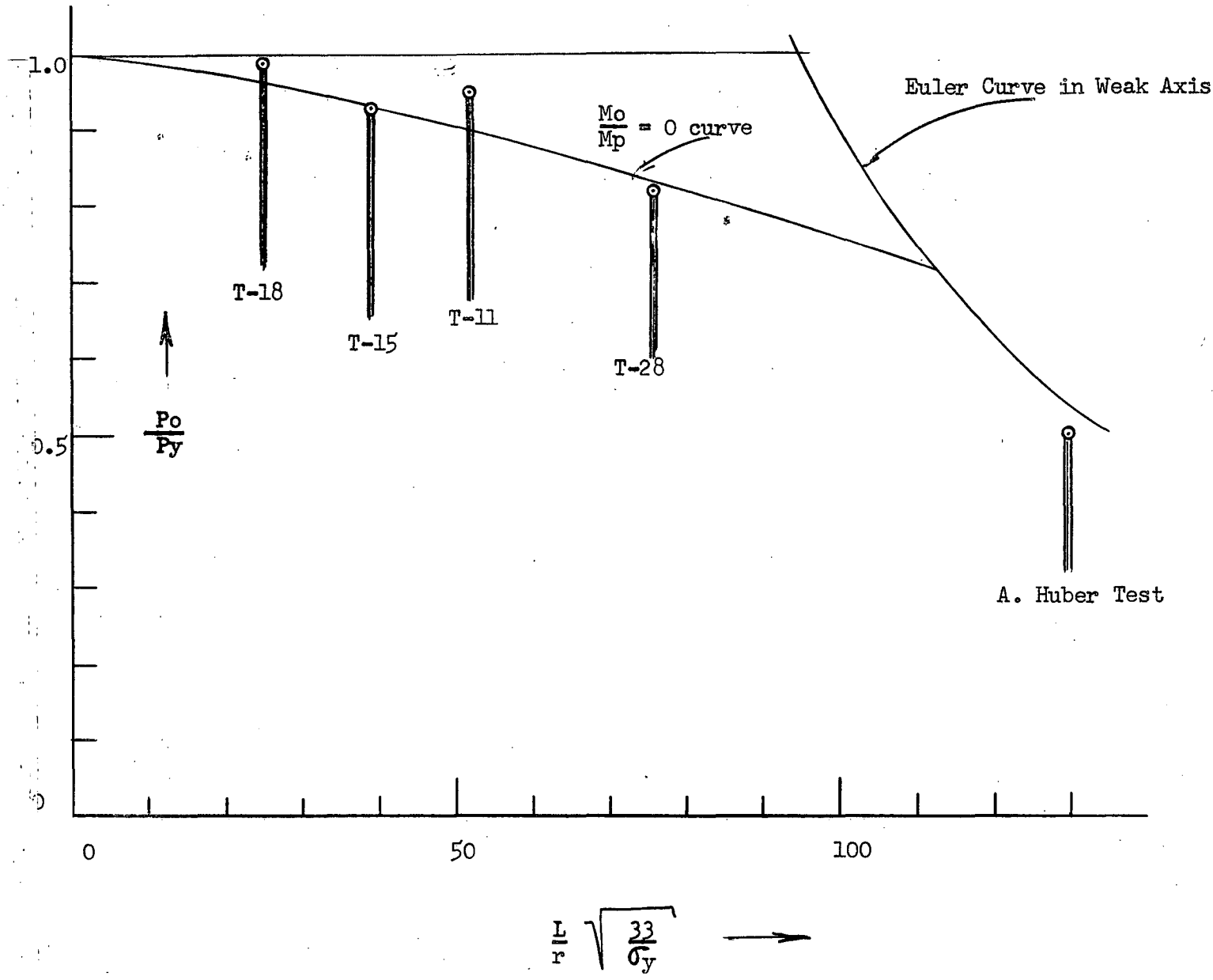

Figure 20

Comparison with Test Results of the Lehigh Test Series

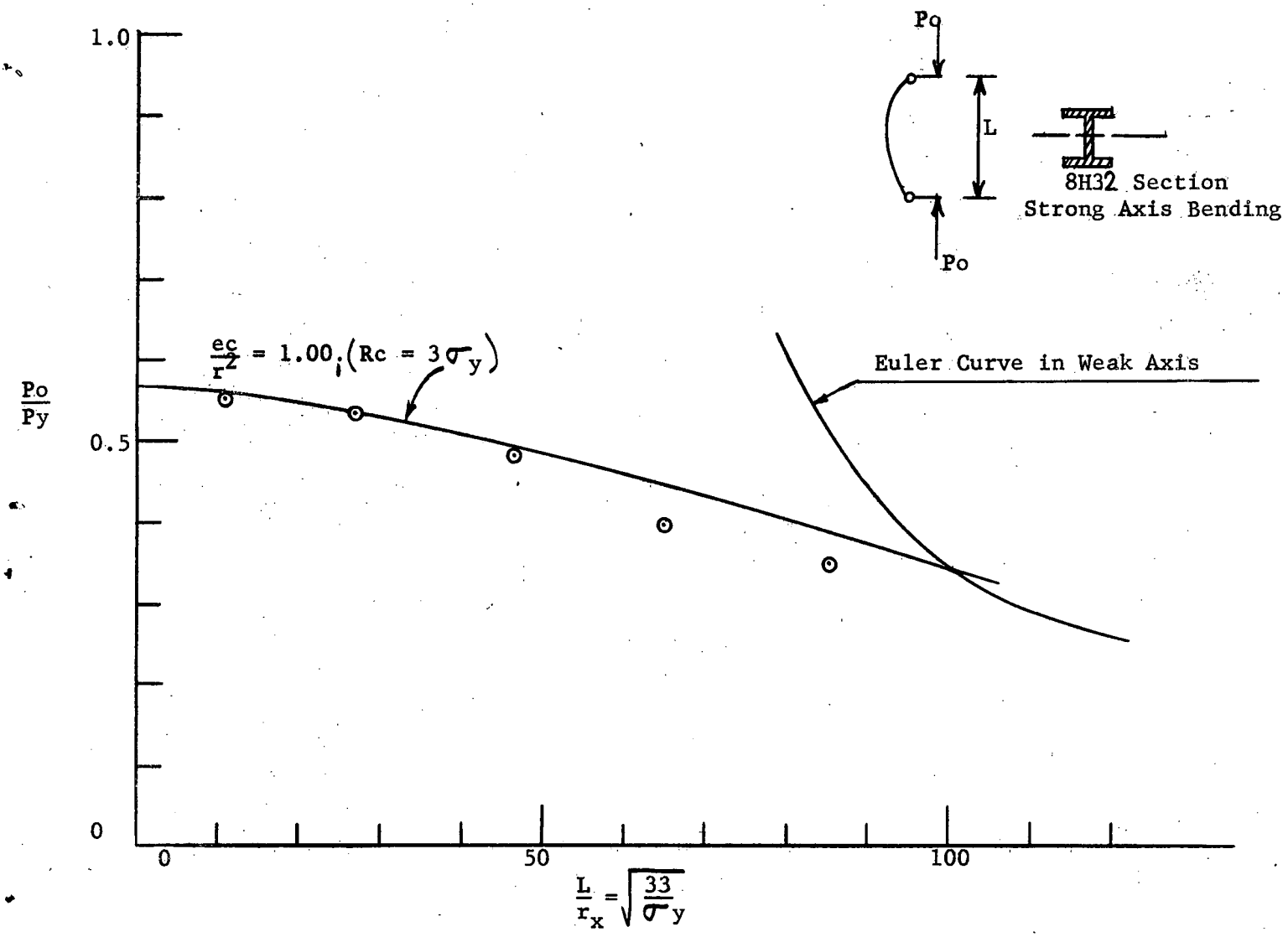

Figure 21

Comparison with Test Results of the Wisconsin Test Series